arXiv:1510.08464v1 [astro-ph.SR] 28 Oct 2015

A Targeted Search for Peculiarly Red L and T Dwarfs in SDSS, 2MASS, and WISE: Discovery of a Possible L7 Member of the TW Hydrae Association

Kendra Kellogg[1,2,6], Stanimir Metchev[1,2], Kerstin Geißler[2], Shannon Hicks[2], J. Davy Kirkpatrick[3], and Radostin Kurtev[4,5]

ABSTRACT

We present first results from a targeted search for brown dwarfs with unusual red colors indicative of peculiar atmospheric characteristics. These include objects with low surface gravities or with unusual dust content or cloud properties. From a positional cross-match of SDSS, 2MASS and WISE, we have identified 40 candidate peculiar early L to early T dwarfs that are either new objects or have not been identified as peculiar through prior spectroscopy. Using low resolution spectra, we confirm that 10 of the candidates are either peculiar or potential L/T binaries. With a $J - K_s$ color of 2.62 $\pm$ 0.15 mag, one of the new objects — the L7 dwarf 2MASS J11193254-1137466 — is among the reddest field dwarfs currently known. Its proper motion and photometric parallax indicate that it is a possible member of the TW Hydrae moving group. If confirmed, it would its lowest-mass (5–6 $M_{\rm Jup}$) free-floating member. We also report a new T dwarf, 2MASS J22153705+2110554, that was previously overlooked in the SDSS footprint. These new discoveries demonstrate that despite the considerable scrutiny already devoted to the SDSS and 2MASS surveys, our exploration of these data sets is not yet complete.

Keywords: binaries: close - brown dwarfs - infrared: stars - stars: peculiar - stars: late-type - stars: individual (2MASS J11193254-1137466)

[1]Western University, Centre for Planetary and Space Exploration, 1151 Richmond St, London, ON N6A 3K7, Canada; kkellogg@uwo.ca, smetchev@uwo.ca

[2]Stony Brook University, Stony Brook, NY 11790, USA

[3]Infrared Processing and Analysis Center, Mail Code 100-22, California Institute of Technology, 1200 E. California Blvd., Pasadena, CA 91125, USA

[4]Instituto de Física y Astronomía, Facultad de Ciencias, Universidad de Valparaíso, Ave. Gran Bretaña 1111, Playa Ancha, Casilla 53, Valparaíso, Chile

[5]Millennium Institute of Astrophysics, Chile

[6]Visiting Astronomer at the Infrared Telescope Facility, which is operated by the University of Hawaii under contract NNH14CK55B with the National Aeronautics and Space Administration.

1. Introduction

Compared to main sequence stars, ultra-cool dwarfs display a wide range of near-infrared colors, even among objects at the same effective temperature or spectral type. The diversity is diagnostic of the unique processes taking place in their molecule- and condensate-rich atmospheres. Effective temperature is the main factor that governs the photospheric appearance of field-aged brown dwarfs, with current understanding pointing to a monotonic correspondence between effective temperature and optical spectral type (Vrba et al. 2004; Golimowski et al. 2004; Looper et al. 2008a).

Cruz et al. (2009) proposed a dimensional extension to the classification scheme for brown dwarfs, by incorporating surface gravity as a second parameter. They adopt a qualitative description of surface gravities—intermediate, low, and very low—based on optical spectral line strengths. Allers & Liu (2013) expanded the classification scheme to the near-IR by adding continuum index measures to classify the absorption strengths of volatile molecules.

Low surface gravities generally contribute to higher dust content in the upper atmospheres of brown dwarfs, making them redder. Analyses of the L and T dwarf population have shown that the optical and near-infrared colors of low-surface gravity objects are readily distinguishable from those of "normal" objects (e.g., Knapp et al. 2004; Cruz et al. 2009; Faherty et al. 2012; Allers & Liu 2013). However, there is also evidence of red brown dwarfs with high dust content without any signatures of youth (Looper et al. 2008b; Kirkpatrick et al. 2010). Their near-IR colors are very similar to those of the young, low-surface gravity objects but their spectra do not have any of the characteristics of youth. That is, peculiarly red brown dwarfs may not necessarily be low-gravity and hence young, but could instead be unusually dusty. As there have not been many unusually red old L dwarfs found, the cause of such dustiness is not well established.

Finding the cause for the enhanced dust content is undoubtedly of interest for understanding the evolution of substellar objects, and the processes that affect the sedimentation and/or condensation of atmospheric dust. It is also crucial for revealing the ages and properties of directly imaged extrasolar planets, most of which exhibit spectral energy distribution (SED) characteristics of both youth and high dust content (e.g., Marley et al. 2012; Bonnefoy et al. 2013). Because isolated brown dwarfs can be scrutinized much more readily than directly imaged extrasolar planets, we stand to potentially learn more about ultra-cool atmospheres from brown dwarfs than we can from exoplanets.

Our understanding of the nature of brown dwarfs with unusual SEDs is presently hindered by the relatively small numbers of such peculiar objects. Until recently, there have been no color-selected searches for peculiar brown dwarfs. Discoveries have been serendipitous, usually a by-product of searches for T dwarfs (Looper et al. 2008a,b; McLean et al. 2007; Burgasser et al. 2004, etc.). Only over the past few years have targeted searches been performed on large-area surveys to specifically seek unusually red objects (e.g., Aller et al. 2013; Gagné et al. 2015).

In view of this, we are conducting an independent program to purposefully seek L and T

dwarfs with unusual optical/near-infrared (near-IR) colors. The goal is to substantially expand the sample of peculiar L and T dwarfs in order to map the full range of their photospheric properties, and to better understand the evolution and content of their atmospheres. We cross-correlated the SDSS, 2MASS, and WISE survey databases to seek candidate peculiar brown dwarfs based solely on photometric criteria. Our first pass through the databases focused mainly on identifying unusually red objects. Most notable among these is one of the reddest L dwarfs ever found (2MASS J11193254-1137466; 2MASS $J - K_s = 2.62 \pm 0.15$ mag). While peculiar L and T dwarfs have until now been found mostly serendipitously in large-scale photometric surveys, we have implemented a systematic approach to find these objects by design. We discuss the selection and prioritization of candidates in Section 2, and their follow-up observations in Section 3. The spectroscopic characterization of the new L and T dwarfs is presented in Section 4. In Section 5 we assess the significance of the findings from our systematic search of peculiar objects in the context of the presently known sample of L and T dwarfs.

2. Candidate Selection

We employ a photometric search for peculiar L and T dwarfs using combined optical (SDSS), near-IR (2MASS) and mid-IR (WISE) fluxes. Our candidate selection expands on the procedure presented in Metchev et al. (2008) and Geißler et al. (2011), which applied joint positional and color constraints to search for T dwarfs in the overlap area of 2MASS and SDSS DR1 (2099 deg^2). We use the ninth Data Release (DR9) from SDSS (Ahn et al. 2012), which has a 14555 deg^2 footprint, encompassing an area 6.9 times larger than the DR1 footprint. The >10-year observational epoch difference between 2MASS and SDSS DR9 prompts us to choose a much larger cross-match radius than was used in the first two studies. We use the Virtual Astronomical Observatory catalog cross-comparison tool[1] and chose a cross-match radius of $16\farcs5$ to maintain sensitivity to objects with proper motions as high as $1\farcs5$ yr^{-1}.

2.1. Selection Criteria

Our magnitude and color selection criteria are summarized below. In the following, all *griz* magnitudes are on the SDSS photometric scale (Lupton et al. 2002), and the 2MASS and WISE magnitudes are on the Vega scale:

1. $z - J > 2.5$ mag;
2. $i - z > 1.5$ mag;
3. $J > 14$ mag;

[1] `http://vao-web.ipac.caltech.edu/applications/VAOSCC/`

4. $z \leq 21$ mag and $z_{err} \leq 0.2$ mag;
5. no $g, r < 23$ mag detection within $1\farcs3$ of the 2MASS coordinate;
6. SDSS object flag setting type = 6 or 3 (point or extended source);
7. 2MASS object flag setting mp_flg = 0 (i.e., not marked as a known minor planet), gal_contam = 0 (i.e., not contaminated by a nearby 2MASS extended source), and ext_key = NULL (i.e., not extended in 2MASS);
8. $H - W2 > 1.2$ mag;
9. $z - J > -0.75(J - K_s) + 3.8$ mag (criterion used only to prioritize follow-up of red outliers).

Our $z - J$ and $i - z$ color cuts (criteria 1 and 2) were chosen to ensure sensitivity to L and T dwarfs, all of which have a steep red optical slope. The $J > 14$ magnitude cutoff was imposed to minimize the large number of candidates representing the cross-identification of a bright star artifact in SDSS (e.g., a filter glint or a diffraction spike, especially near saturated stars) with the (unsaturated) image of the same star in 2MASS. Criterion 4 was chosen to ensure detection in SDSS with at least a moderate SNR.

Our $16\farcs5$ matching radius commonly resulted in multiple matches of nearby faint SDSS objects to the same, brighter 2MASS object. Each of these individual matches would nominally satisfy the color and magnitude selection criteria, since the faint SDSS photometry would be paired with the brighter 2MASS photometry. However, visual inspection clearly demonstrated that the SDSS and 2MASS objects were distinct, and that the actual object in SDSS that positionally matched the 2MASS object was not nearly as red, and so did not satisfy the $z - J > 2.5$ mag criterion. Therefore, we discarded any object that had a g-band detection (i.e. $g \leq 23$ mag and likely a star) in the SDSS catalog within $1\farcs3$ (the angular resolution of SDSS) of the original 2MASS coordinates (criterion 5). This removed $\sim$86% of the candidate sample.

The SDSS object flag restrictions (criterion 6) ensure that the identified candidates are not known artifacts or flux measurements of the blank sky in SDSS. The SDSS morphological star-galaxy separation is $< 97\%$ accurate for $r \geq 21$ mag (Yasuda et al. 2001) so we include both star and galaxy object types in this criterion in case our faint brown dwarfs were mis-classified. We also wanted to ensure that they are not known minor planets, extended or contaminated by nearby extended sources in 2MASS (criterion 7).

To make sure that all of the objects in our candidate list were real objects, we cross-matched our list with the WISE All-Sky Data Release using the SDSS coordinates. Our objects are expected to be detected in the WISE $W1$ band because outside of the galactic plane the $W1$ SNR = 5 level corresponds to $\lesssim 16.8$ mag.[2] This matches the 2MASS K_s flux limit at high galactic latitude, especially since L and T dwarfs have positive $K_s - W1$ colors. A radius of $16\farcs5$ was again chosen for this cross-match. An additional color cut was applied on $H - W2$ (criterion 8) in order to select only L and T dwarfs (based the color-spectral type relations from Kirkpatrick et al. 2011). This

[2] http://wise2.ipac.caltech.edu/docs/release/allsky/expsup/sec6_3a.html

removed ∼74% of the remaining sample.

Finally, we visually inspected the images of remaining candidates using the Infrared Science Archive Finder Chart service[3] and removed objects that were contaminated by nearby extended sources in SDSS. This eliminated approximately 22% of the remaining candidate sample leaving us with 314 candidates (Figure 1a).

2.2. Prioritization of Peculiar Objects

Since our goal was to select unusually red brown dwarfs in the absence of spectral type information, an additional color criterion (9) was set in order to prioritize ed objects. To decide the form of the color criterion, we first analyzed the spectra of L and T dwarfs in the SpeX Prism Archive[4] by forming synthetic photometry over various red-optical and near-IR bandpasses. These L and T dwarfs with archival SpeX data formed our control sample, based on which we designed our $z - J$ vs. $J - K_s$ criterion 9 (Figure 1b).

Given available spectral type information, the unusually red objects in the control sample were set to be those for which the $J-K_s$ color was >2-σ redder than the median for the spectral subtype. The medians and standard deviations of the $J - K_s$ colors of M8-T8 dwarfs were adopted from Faherty et al. (2009; M8-M9 and T0-T9) and from Faherty et al. (2013; L0-L9). The unusually red objects in the control sample are shown with red symbols in Figure 1b. The number of objects from our sample that passed this criteria was 178.

The color prioritization did not streamline our observational follow-up strategy significantly, as the scatter in colors among spectral types is larger than the scatter at any given spectral type. Nonetheless, we did observe the reddest candidates whenever possible, and included observations of lower-priority targets only as necessary.

3. Spectroscopic Observations and Data Reduction

Once our candidates were selected, we performed follow-up spectroscopic observations of 40 of the objects (∼13% of the total candidate sample; 22 high priority and 18 lower priority) using the SpeX instrument (Rayner et al. 2003) on the NASA Infrared Telescope Facility (IRTF) and the Folded-port InfraRed Echellette (FIRE) instrument (Simcoe et al. 2008) on the Magellan Baade telescope. Conditions were photometric on most nights, except on August 3, 2011, April 18, 2012, April 19, 2012, and July 14, 2012, when there was scattered cirrus. All reduction of the low-resolution spectra (SpeX and FIRE LD) was done in Interactive Data Language (IDL).

---

[3] http://irsa.ipac.caltech.edu/applications/FinderChart/

[4] http://pono.ucsd.edu/~adam/browndwarfs/spexprism/

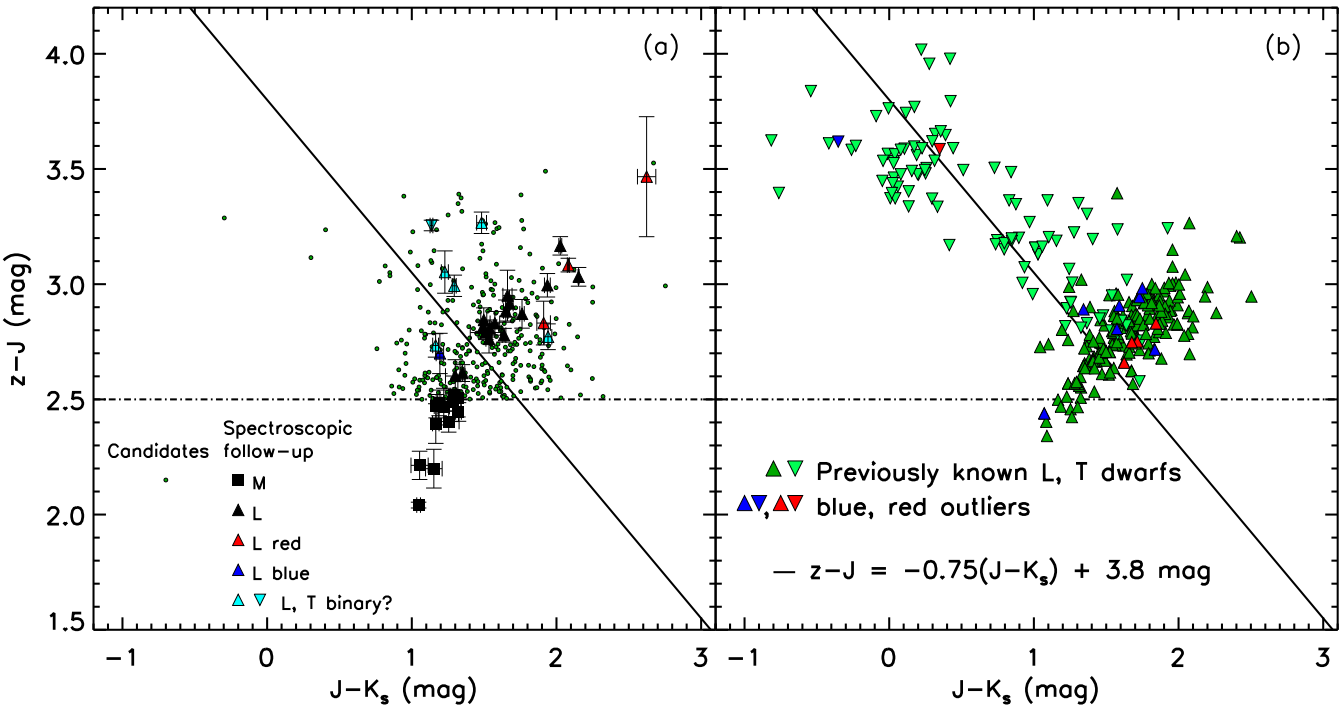

Fig. 1.— (a) Photometric color-color diagram of all L and T dwarf candidates redder than $z-J=2.5$ mag (green dots) identified in our SDSS-2MASS-WISE cross-match. All other symbols (squares - M dwarfs; upwards triangles - L dwarfs; downwards triangle - T dwarf) represent the synthetic colors of the candidates followed up with spectroscopic observations so far. The black symbols are "normal" objects and the red and blue symbols are objects that we have identified as peculiar or binary. Objects redder than the $z-J=-0.75(J-K_s)+3.8$ mag line are candidate peculiarly red L and T dwarfs and were prioritized for spectroscopic follow-up. (b) SDSS/2MASS synthetic color-color diagram of L and T dwarfs from the SpeX Prism Archive (upwards and downwards triangles, respectively). The $z-J$, and $J-K_s$ colors were formed synthetically from the SpeX spectra. Two-sigma red and blue photometric color outliers are indicated by red and blue symbols, respectively. The $z-J=-0.75(J-K_s)+3.8$ mag line was designed to select the photometric red outliers.

3.1. IRTF/SpeX

The majority of our follow-up observations were taken using the SpeX spectrograph on the IRTF. The broad, simultaneous wavelength coverage (0.8–2.5 μm) of SpeX and its location in the northern hemisphere are ideal for follow-up of SDSS-identified candidates. These spectra were obtained between 2011 August and 2013 June. The observations were taken in prism mode either with the $0\farcs8 \times 15\farcs0$ or with the $1\farcs6 \times 15\farcs0$ slit, resulting in resolutions of $R \sim$150 and $\sim$75, respectively. The slit orientation was maintained to within 20° of the parallactic angle for all targets. We used a standard A-B-B-A nodding sequence along the slit to record object and sky spectra. Individual exposure times were either 60 s or 180 s per pointing. The shorter exposure times allowed us to better subtract the sky-glow under changing atmospheric conditions. Standard stars were used for flux calibration and telluric correction. Flat-field and argon lamps were observed immediately after each set of target and standard star observations for use in instrumental calibrations. Observation epochs and instrument settings for each science target are given in Table 1.

All reductions of the data taken with SpeX were carried out with the SPEXTOOL package version 3.4 (Cushing et al. 2004; Vacca et al. 2003), using a weighted profile extraction approach (Horne 1986; Robertson 1986). The aperture widths were set to be the radius at which the spatial profile dropped to $\sim$5% of the peak flux value to ensure no contamination from background noise; the background regions were chosen to begin at the edge of the PSF radius (i.e., beyond 2.5 pixels = $0\farcs375$). A constant value was fit to the background and subtracted from the spectrum. The individual extracted and wavelength calibrated spectra from a given sequence of observations, each with their own A0 standard, were then scaled to a common median flux and median-combined using X_COMBSPEC. The combined spectra were corrected for telluric absorption and flux-calibrated using the respective telluric standards with X_TELLCOR. All calibrated sets of observations of a given object were median combined to produce the final spectrum. The reduced spectra were smoothed to the instrumental resolution corresponding to the chosen slit width, using the Savitzky-Golay smoothing kernel (Press et al. 1992).

Table 1. SpeX Observations

Identifier (J2000)	Date (UT)	2MASS J (mag)	Slit Width (arcsec)	Exposure (min)	A0 Calibrator
2MASS J08095903+4434216	2011 Dec 31	16.44	0.8	24	HD 75135
2MASS J09572983+4624177	2013 Jun 06	16.25	1.6	24	HIP 53735
2MASS J10020752+1358556	2013 Jun 07	17.19	1.6	32	HIP 35735, HIP 54815
2MASS J11193254-1137466	2013 Jun 06	17.29	1.6	16	HIP 53735
... [a]	2013 Jun 07	17.29	1.6	8	HIP 54815
2MASS J11260310+4819256	2013 Jun 07	17.20	1.6	24	HIP 54815, HIP 56147
2MASS J13043568+1542521	2013 Jun 06	17.32	1.6	70	HIP 68209, HIP 68868
2MASS J13431670+3945087	2011 Dec 31	16.16	0.8	16	HD 125798
2MASS J14025564+0800553	2013 Jun 07	16.84	1.6	160	HIP 68868, HIP 116886
2MASS J16005759+3021571	2011 Aug 02	16.97	0.8	54	HD 153650
2MASS J16094569+1426422	2011 Aug 03	16.84	0.8	60	HD 152531
2MASS J16091143+2116584	2011 Aug 02	16.96	0.8	60	HD 153650
2MASS J16135698+4019158	2012 Apr 19	17.05	0.8	48	HD 151353
2MASS J16231308+3950419	2012 Apr 18	16.97	0.8	60	HD 165623
2MASS J16242936+1251451	2011 Aug 03	16.26	0.8	36	HD 152531
2MASS J16304999+0051010	2012 Jul 14	16.00	0.8	12	HD 157359
2MASS J16322360+2839567	2012 Apr 18	16.63	0.8	48	HD 158261
2MASS J16360752+2336011	2012 Jul 14	16.88	0.8	12	HD 157359
2MASS J16370238+2520386	2011 Aug 03	16.50	0.8	36	HD 157359
2MASS J16403870+5215505	2012 Apr 19	17.22	0.8	60	HD 155838
2MASS J16410015+1335591	2011 Aug 03	16.90	0.8	48	HD 157359
2MASS J16470847+5120088	2012 Apr 19	17.03	0.8	48	HD 155838
2MASS J16592987+2055298	2012 Jul 15	16.33	1.6	90	HD 164728
2MASS J17081563+2557474	2011 Aug 02	16.42	0.8	48	HD 164728
2MASS J17145224+2439024	2012 Jul 14	16.84	0.8	12	HD 165623
2MASS J17161258+4125143	2011 Aug 03	16.75	0.8	36	HD 165623, HD 165622
... [a]	2012 Jul 15	16.75	1.6	36	HD 165623
2MASS J17251557+6405005	2012 Jul 15	16.81	1.6	24	HD 165622
2MASS J17373467+5953434	2012 Apr 19	16.88	0.8	60	HD 166639
2MASS J21050130-0533505	2011 Aug 03	16.42	0.8	36	HD 209051
2MASS J21111559-0543437	2011 Aug 03	16.09	0.8	36	HD 209051
2MASS J21115335-0644172	2011 Aug 02	16.90	0.8	60	HD 209051
2MASS J21203483-0747378	2011 Aug 02	16.82	0.8	60	HD 210253
2MASS J21243864+1849263	2013 Jun 06	17.03	1.6	56	HIP 53735, HIP 68209, HIP 68868
2MASS J21392224+1124323	2011 Aug 03	16.49	0.8	48	HD 210265
... [a]	2011 Dec 31	16.49	0.8	36	HD 210265
... [a]	2012 Jul 15	16.49	0.8	48	HD 210265

3.2. Magellan/FIRE

Two of the 40 total candidates were observed using the FIRE spectrograph on the 6.5 m Magellan telescope. The observations of these objects were taken in the low-dispersion (LD) mode with the $0\farcs6 \times 50\farcs0$ longslit resulting in a resolution of ∼400. We used a standard A-B-B-A nodding sequence along the slit to record object and sky spectra. Individual exposure times ranged from 31.7–126.8 s per pointing, depending on the brightness of the object. Standard stars were used for flux calibration and telluric correction. We used optimal gain settings of 1.2 e^-/DN and 3.8 e^-/DN for the science targets and 3.8 e^-/DN for the standards as suggested in the FIRE observing manual[5]. Illumination and appropriate pixel flats were observed either at the beginning or the end of the night and a neon-argon lamp was observed immediately after each set of target and standard star observations for use in instrumental calibrations. All science and telluric observations were taken using the sample-up-the-ramp (SUTR) readout mode whereas all calibration observations were taken in Fowler 1 mode due to the shortness of exposure times. Observation epochs and instrument settings for each target are given in Table 2.

The FIRE low-dispersion spectra were reduced using the FIREHOSE Low Dispersion package which evolved from the optical echelle reduction software package MASE (Bochanski et al. 2009). The spectra were extracted using the optimal extraction approach with the aperture radius being the PSF radius (usually ∼3 pixels = $0\farcs45$) which was then masked to prevent biasing to the sky model. A local background was modeled using a basis spline (i.e., piecewise polynomial) fit to the masked profile and subtracted from the spectra which were subsequently extracted using a weighted profile extraction approach (Horne 1986). The extracted spectra were wavelength-calibrated and each set of observations were median-combined. The combined spectra were corrected for telluric absorption and flux-calibrated with their associated A0 calibration star. All calibrated sets of observing sequences of a given object were median combined to produce a final spectrum. The reduced spectra were smoothed, using the IDL Savitzky-Golay smoothing algorithm, to the same resolution as the SpeX standards for comparison.

3.3. Synthetic Photometry

While comparing the 2MASS colors of our L and T dwarf candidates to their spectra, we noticed that in a significant fraction of cases the 2MASS colors were too red compared to the spectra. All of our objects were flux-calibrated with A0 stars with known $B-V$ colors, observed at similar airmasses, so we had no reason to suspect a chromatic effect in our flux calibration. Instead, the reason for the discrepancy was traced to flux over-estimation bias at low SNR in 2MASS.

Our objects are faint and often near the SNR = 5 detection limit of 2MASS in the J-band

[5]http://web.mit.edu/~rsimcoe/www/FIRE/ob_manual.htm

Table 1—Continued

Identifier (J2000)	Date (UT)	2MASS J (mag)	Slit Width (arcsec)	Exposure (min)	A0 Calibrator
2MASS J22153705+2110554	2013 Jun 07	16.00	1.6	72	HIP 116886
2MASS J22483513+1301453	2011 Dec 31	16.82	0.8	28	HD 220184
... [a]	2012 Jul 14	16.82	1.6	36	HD 220184
... [a]	2012 Jul 15	16.82	0.8	24	HD 210265
2MASS J23023319-0935188	2012 Jul 15	16.80	0.8	60	HD 222903
2MASS J23322678+1234530	2013 Jun 06	16.89	1.6	42	HIP 68868
2MASS J23443744-0855075	2011 Aug 02	16.77	0.8	60	HD 2717

[a]Repeat observations of the same object, combined with the previous data.

Table 2. FIRE Observations

2MASS ID (J2000)	Date (UT)	J (mag)	Dispersion Mode	Slit Width (arcsec)	Gain (e^-/DN)	Exposure (min)	A0 Calibrator
2MASS J07483864+1743329	2012 Mar 21	16.27	Long Slit	0.60	3.8	4.2	HD 57450
2MASS J16110632+0025469	2012 Mar 21	17.02	Long Slit	0.60	1.2	16.9	HD 153940

filter. The greater noise near the detection limit means that objects that would normally be below the limit have a finite chance of appearing brighter because of statistical variations. The effect enhances the number of faint objects with low SNR in a flux-limited survey, becoming increasingly important at SNR < 10 (Cutri 2006). Because all of our objects are faint and red, their 2MASS J-band magnitudes preferentially suffer from this bias, resulting in redder than expected $z - J$ colors. This effect is particularly large in the case of the few faint M-dwarfs that entered our sample because of their biased photometric colors (section 4.1). Figure 2 shows how the synthetic colors compare to the photometric colors as a function of the photometric J-band SNR for both $z - J$ and $J - K_s$. Indeed, at lower SNR, the $z - J$ photometric colors are on average redder than their synthetic colors while the $J - K_s$ photometric colors are on average slightly bluer.

For the remainder of our analysis we use only synthetic SDSS z and 2MASS JHK_s magnitudes for our candidates and for previously known objects with SpeX Prism Archive spectra. The errors on the synthetic photometry in Table 3 are standard errors derived from the scatter among the continuum slopes of the individual 60 s or 180 s-exposure spectra of our targets and their corresponding standard stars. These errors incorporate systematic uncertainties from potential chromatic slit losses should the targets have been imperfectly positioned on the slit.

4. Spectral Classification Results

We estimate spectral types for our objects by comparing them to spectra of brown dwarfs available from the SpeX Prism Archive[6]. When our spectra don't match any of the normal brown dwarf spectra, we compare to other unusual spectra. In this way, we are able to assess potential spectroscopic peculiarities that may not be evident from the colors alone. Finally, following the approach of Burgasser (2007) and Burgasser et al. (2010), we form combination templates from the standards to assess whether any of our objects might be best fit as unresolved binaries. For spectral comparison to standard L and T dwarfs we used χ^2 minimization over the 0.95-1.35 μm wavelength range. To assess candidate binarity we compare our spectra to combinations of L and/or T dwarf doubles over the entire 0.8-2.5 μm range, as detailed in Section 4.3. Table 3 lists the determined spectral types, the characteristics of each object, and the peculiarities of our objects determined from both colors and a detailed analysis of their spectra. All of our spectra are shown in Figure 3.

We determined that our candidate list of 40 observed objects includes 13 M dwarfs, 26 L dwarfs, and 1 T dwarf. Of these, 10 were previously known and suspected to be L dwarfs but did not have any published near-IR spectra. The remaining 30 are new, including the T dwarf. Ten of the 27 L and T dwarfs are either peculiar (4) or possible unresolved binaries (6).

[6]Kirkpatrick et al. (2010), Burgasser et al. (2010), Burgasser et al. (2008), Burgasser et al. (2007), Looper et al. (2007), Burgasser et al. (2006b), Chiu et al. (2006), Reid et al. (2006), and Burgasser et al. (2004)

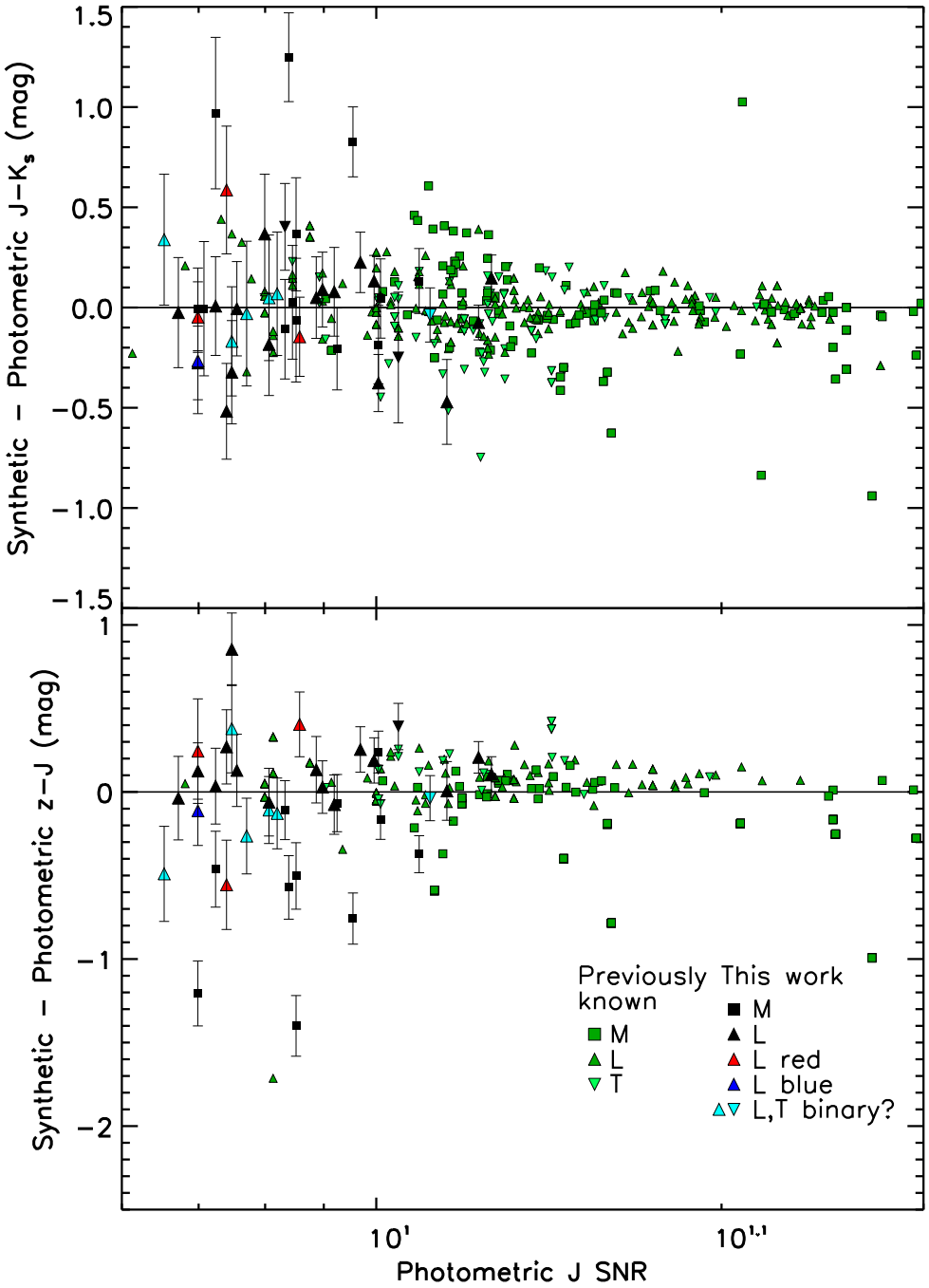

Fig. 2.— Difference in synthetic vs photometric $J - K_s$ and $z - J$ colors for M, L and T dwarfs from the SpeX Prism Archive (green symbols) and for objects from this work (all other colored symbols). The black symbols are "normal" objects and the blue and red symbols are objects that we have identified as peculiar or binary. Fewer objects appear in the $z - J$ comparison figure (lower panel) because not all SpeX Archive objects are in the SDSS database.

Table 3. Results from Spectroscopic Classification and Synthetic Photometry

2MASS ID (J2000)	IR SpT	Interpretation (from spectrum)	z (mag)	J (mag)	H (mag)	K_s (mag)	Disc. Pub.	>1σ Color Outlier	>2σ Color Outlier
				High Priority					
07483864+1743329	L5		...[a]	... [b]	...	...	1		
08095903+4434216	L7		19.25 ± 0.09	16.22 ± 0.05	14.94 ± 0.05	14.07 ± 0.05	2	+	
09572983+4624177	L6		19.78 ± 0.08	16.62 ± 0.06	15.39 ± 0.06	14.59 ± 0.06	7	+	
10020752+1358556	L7 pec	L7+T8?	20.49 ± 0.10	17.72 ± 0.08	16.56 ± 0.06	15.78 ± 0.07			
11193254-1137466	L7 red	young	20.69 ± 0.30	17.23 ± 0.12	15.70 ± 0.08	14.60 ± 0.10			+
11260310+4819256	L5		20.07 ± 0.11	17.20 ± 0.07	16.14 ± 0.06	15.44 ± 0.06			
13043568+1542521	T0 pec	L6+T6?	20.50 ± 0.09	17.24 ± 0.08	16.37 ± 0.06	15.76 ± 0.08			
13431670+3945087	L5		19.02 ± 0.10	16.02 ± 0.08	14.84 ± 0.07	14.08 ± 0.07	3		
14025564+0800553	T2 pec	L8+T5?	20.30 ± 0.09	17.31 ± 0.07	16.51 ± 0.04	16.01 ± 0.06	5	+	
16005759+3021571	L5		20.25 ± 0.10	17.33 ± 0.07	16.30 ± 0.06	15.66 ± 0.07			
16094569+1426422	L4		19.70 ± 0.08	16.92 ± 0.06	15.93 ± 0.06	15.28 ± 0.06			
16091143+2116584	L2		20.02 ± 0.10	17.19 ± 0.09	16.25 ± 0.08	15.62 ± 0.09	1		
16135698+4019158	L5 red	old/dusty	20.29 ± 0.13	17.46 ± 0.10	16.30 ± 0.06	15.54 ± 0.10		+	
16470847+5120088	M9		19.58 ± 0.10	17.10 ± 0.05	16.36 ± 0.06	15.91 ± 0.06			
16592987+2055298	M9		20.14 ± 0.13	17.75 ± 0.08	17.06 ± 0.06	16.58 ± 0.07			
17081563+2557474	L5 red	young	20.00 ± 0.08	16.92 ± 0.04	15.68 ± 0.05	14.84 ± 0.04		+	
17161258+4125143	L4		19.77 ± 0.16	16.82 ± 0.09	15.83 ± 0.09	15.16 ± 0.08			
17373467+5953434	L5 pec	L4+T5?	20.80 ± 0.14	17.75 ± 0.08	16.97 ± 0.07	16.52 ± 0.07	6		−
21203483-0747378	L2		19.97 ± 0.08	17.17 ± 0.06	16.24 ± 0.05	15.68 ± 0.05	6		
21243864+1849263	L9		20.15 ± 0.09	17.27 ± 0.05	16.18 ± 0.05	15.62 ± 0.06			
22153705+2110554	T1 pec	T0+T2?	19.48 ± 0.07	16.22 ± 0.07	15.45 ± 0.06	15.09 ± 0.05			
23322678+1234530	T0 pec	L5+T5?	19.66 ± 0.10	16.92 ± 0.08	16.20 ± 0.07	15.76 ± 0.06			−
				Lower Priority					
16110632+0025469	M9		...[a]	... [b]	...	...	4		
16231308+3950419	L3		20.16 ± 0.08	17.35 ± 0.06	16.42 ± 0.06	15.81 ± 0.05			
16242936+1251451	M9		19.20 ± 0.06	16.68 ± 0.06	15.88 ± 0.04	15.39 ± 0.06	5		
16304999+0051010	L2		18.40 ± 0.11	15.64 ± 0.07	14.74 ± 0.06	14.11 ± 0.07			
16322360+2839567	L1		19.90 ± 0.12	17.30 ± 0.12	16.50 ± 0.10	16.00 ± 0.10			
16360752+2336011	L1		19.61 ± 0.08	17.00 ± 0.07	16.16 ± 0.06	15.65 ± 0.06	5		
16370238+2520386	L4		19.95 ± 0.10	17.10 ± 0.08	16.18 ± 0.07	15.61 ± 0.06		−	
16403870+5215505	M9		20.37 ± 0.09	17.97 ± 0.11	17.19 ± 0.08	16.72 ± 0.11			
16410015+1335591	L2		20.27 ± 0.08	17.48 ± 0.14	16.56 ± 0.10	15.97 ± 0.14			
17145224+2439024	M9		19.17 ± 0.12	16.67 ± 0.08	15.86 ± 0.07	15.35 ± 0.07			

Table 3—Continued

2MASS ID (J2000)	IR SpT	Interpretation (from spectrum)	z (mag)	J (mag)	H (mag)	K_s (mag)	Disc. Pub.	$>1\sigma$ Color Outlier	$>2\sigma$ Color Outlier
17251557+6405005	L2 pec	blue	20.10 ± 0.13	17.40 ± 0.08	16.66 ± 0.07	16.20 ± 0.07	1		–
21050130-0533505	M7		18.36 ± 0.06	16.32 ± 0.06	15.65 ± 0.06	15.28 ± 0.06			
21111559-0543437	M9		18.94 ± 0.09	16.46 ± 0.08	15.67 ± 0.08	15.17 ± 0.07			
21115335-0644172	M9		19.83 ± 0.08	17.38 ± 0.06	16.60 ± 0.06	16.06 ± 0.07			
21392224+1124323	M8		19.74 ± 0.13	17.54 ± 0.10	16.81 ± 0.08	16.39 ± 0.10			
22483513+1301453	M9		19.61 ± 0.12	17.14 ± 0.09	16.38 ± 0.07	15.92 ± 0.08			
23023319-0935188	M7		19.63 ± 0.10	17.41 ± 0.10	16.75 ± 0.07	16.36 ± 0.10			
23443744-0855075	M9		19.43 ± 0.10	16.96 ± 0.06	16.24 ± 0.04	15.79 ± 0.05			

Note. — Determination of color outliers came from comparing synthetic $J - K_s$ colors to average $J - K_s$ colors for M8-M9 and T0-T8 spectral types from Faherty et al. (2009) and for L0-L9 spectral types from Faherty et al. (2013). Positives and negatives indicated whether the object was above or below the average, respectively. [1]Zhang et al. (2009), [2]Knapp et al. (2004), [3]Kirkpatrick et al. (2000), [4]Schmidt et al. (2010), [5]Chiu et al. (2006), [6]Geißler et al. (2011), [7]Luhman & Sheppard (2014).

[a]FIRE spectra do not cover the entire SDSS z-band.

[b]Target and standard observations were taken with different gain settings so individual JHK$_s$ magnitudes are not reported.

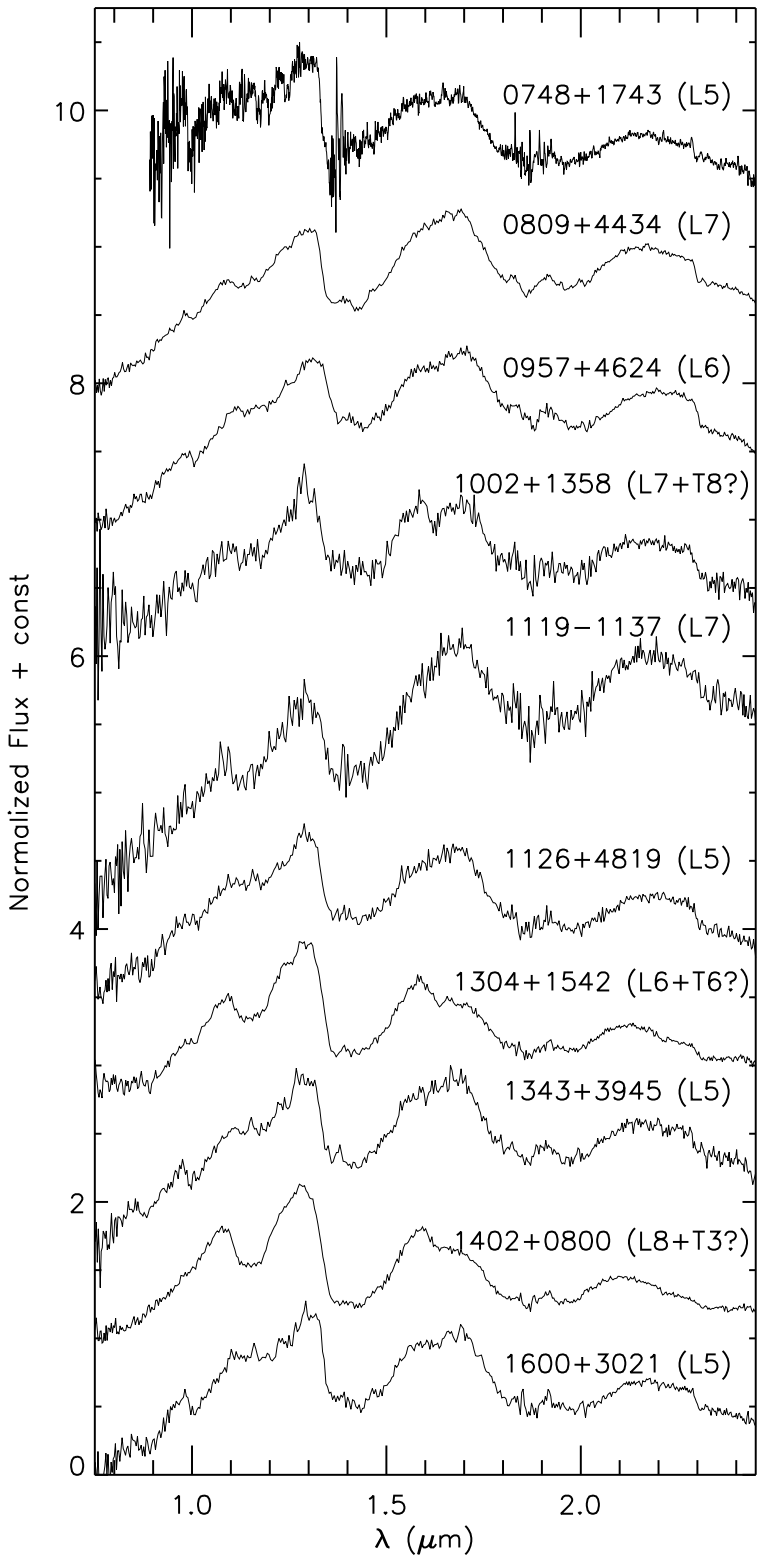

Fig. 3.— FIRE (0748+1743, 1611+0025; R ∼400) and SpeX (all the rest; R ∼75-150) spectra of all of our reported ultra-cool dwarfs in order of right ascension. Spectral types are given in parentheses.

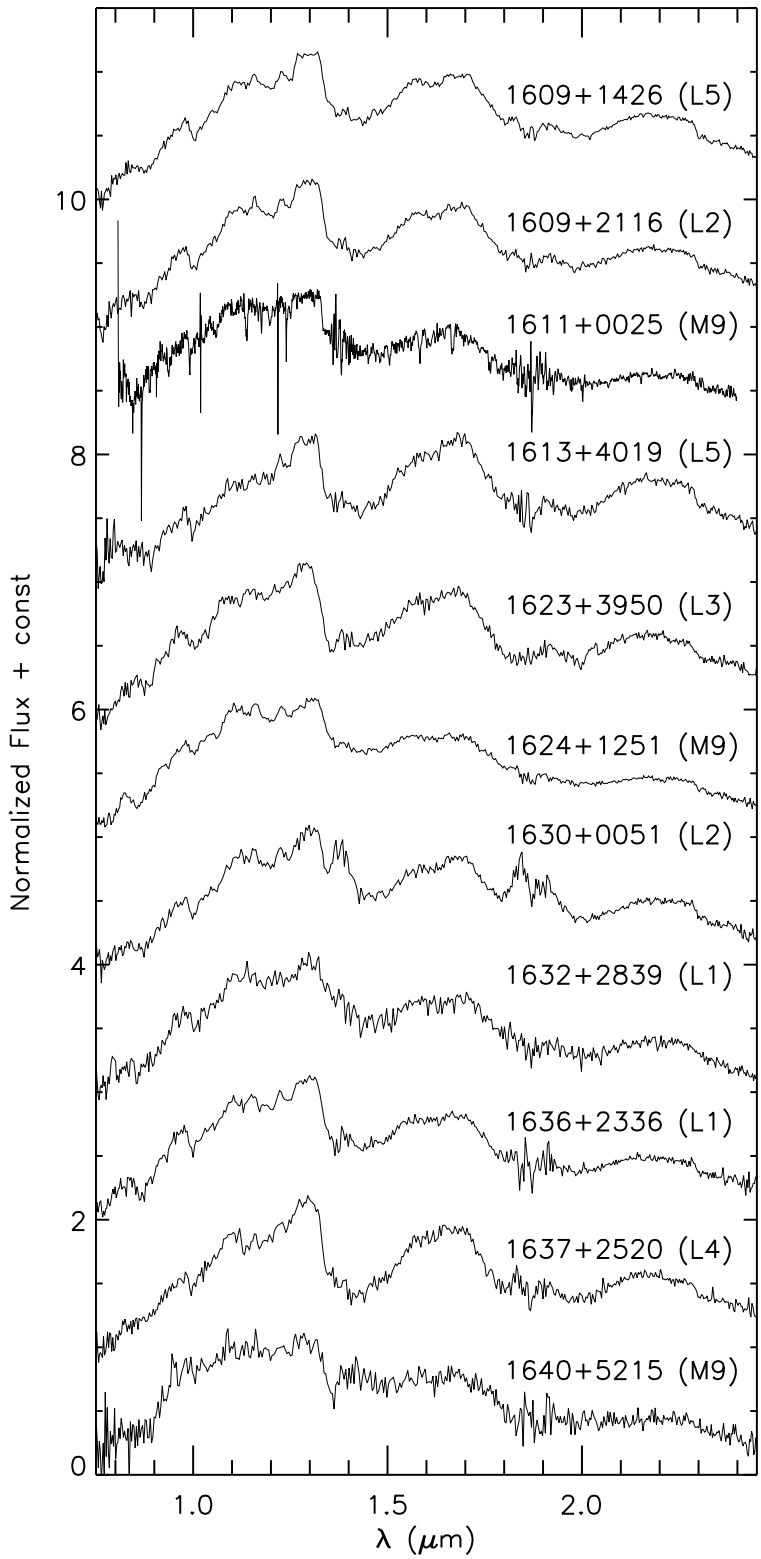
1609+1426 (L5)
1609+2116 (L2)
1611+0025 (M9)
1613+4019 (L5)
1623+3950 (L3)
1624+1251 (M9)
1630+0051 (L2)
1632+2839 (L1)
1636+2336 (L1)
1637+2520 (L4)
1640+5215 (M9)
Normalized Flux + const
λ (μm)
0
2
4
6
8
10
1.0
1.5
2.0

Fig. 3 (cont).—

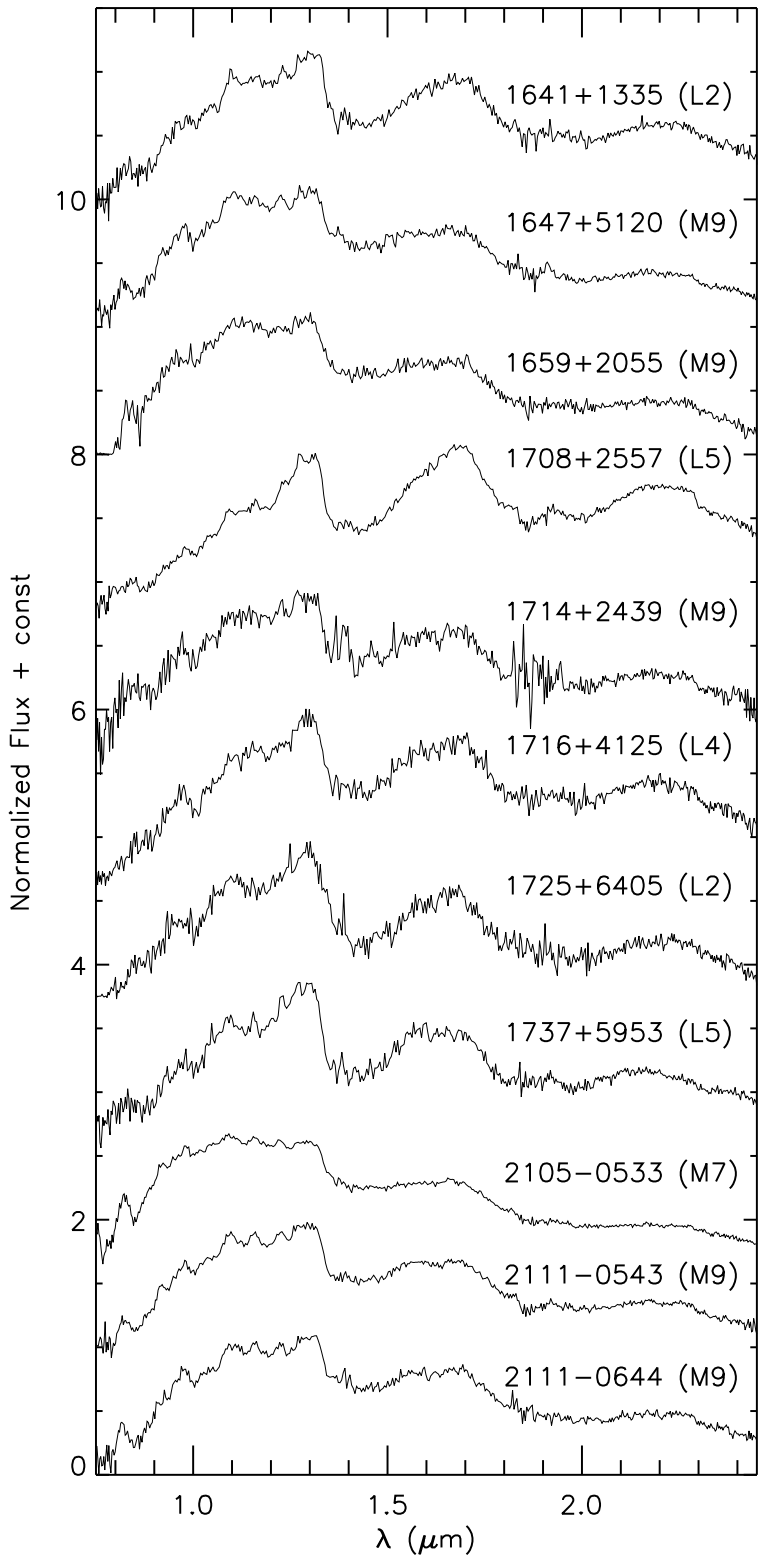
1641+1335 (L2)
1647+5120 (M9)
1659+2055 (M9)
1708+2557 (L5)
1714+2439 (M9)
1716+4125 (L4)
1725+6405 (L2)
1737+5953 (L5)
2105−0533 (M7)
2111−0543 (M9)
2111−0644 (M9)
Normalized Flux + const
λ (μm)
0
2
4
6
8
10
1.0
1.5
2.0

Fig. 3 (cont).—

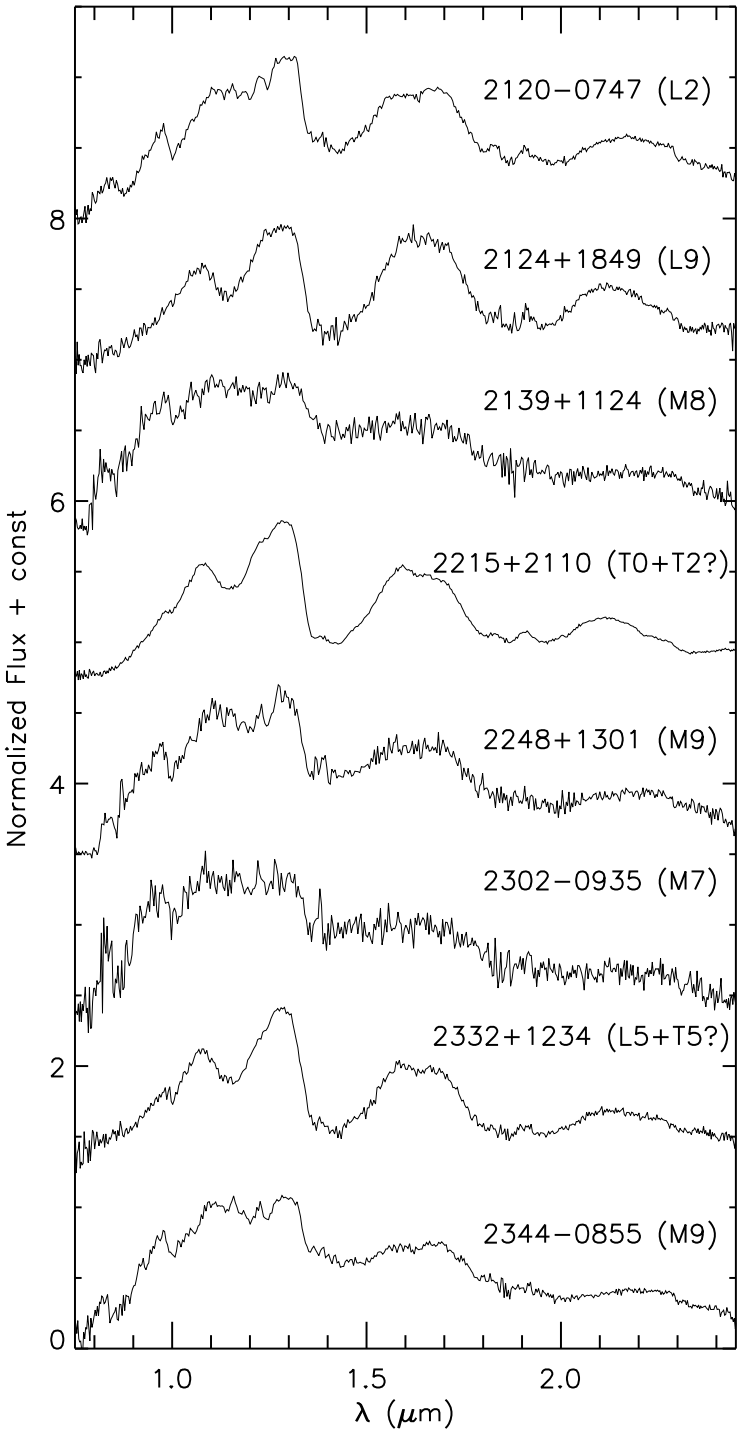
2120−0747 (L2)
2124+1849 (L9)
2139+1124 (M8)
2215+2110 (T0+T2?)
2248+1301 (M9)
2302−0935 (M7)
2332+1234 (L5+T5?)
2344−0855 (M9)
Normalized Flux + const
λ (μm)
0
2
4
6
8
1.0
1.5
2.0

Fig. 3 (cont).—

The newly classified M, L, and T dwarfs are plotted on the $z-J$ vs. $J-K_s$ color-color diagram in Figure 1a, where we have used the synthetic colors integrated from the spectra. We find that in a few cases the synthetic $z-J$ colors are bluer than 2.5 mag. As discussed in Section 3.3, this is likely the result of flux over-estimation bias for these faint targets, mostly in the 2MASS J-band. We discuss the normal, peculiar, and candidate binary ultra-cool dwarfs in our sample below.

A handful of objects have synthetic colors that are bluer than the $z-J=2.5$ mag color selection criterion. The SDSS and 2MASS photometry had suggested that they were redder than $z-J=2.5$ mag. However, their photometric SNRs from 2MASS and/or SDSS were low (see §3.3), and the synthetic photometry indicates that they are in fact bluer.

4.1. Normal Ultra-cool Dwarfs

We classify 17 of our candidates as normal L dwarfs, i.e., they do not have any readily apparent peculiarities based on their comparison to SpeX spectral standards. These objects are presented as black upward-triangles in Figure 1a. We find that a further 13 candidates are M7–M9 dwarfs. These were included in our program likely because the $i-z$ and $z-J$ colors of late-M dwarfs are close to the limits of our color selection criteria (Section 2.1), and because they may have been subject to flux-overestimation bias at J band (Section 3.3).

4.2. Peculiar L Dwarfs

Various absorption features in the near-infrared are gravity-sensitive, hence, the low-gravity of young brown dwarfs will result in line strengths that differ from those in older objects (e.g., Lucas et al. 2001; Gorlova et al. 2003; McGovern et al. 2004; Allers et al. 2007; Lodieu et al. 2008; Rice et al. 2010; Allers & Liu 2013). Some of these features include the Na I (1.138 and 1.141 μm) and K I (1.169 and 1.178 μm, 1.244 and 1.253 μm) doublets, FeH (bandheads at 0.990 μm and 1.194 μm), and VO (1.05–1.08 μm and 1.17–1.22 μm). Alkali lines are weaker at low gravity because of decreased pressure broadening. In low-resolution spectra these lines are often blended with other molecular features so we can not obtain accurate measurements of their strengths. Metal hydride molecular features are also weaker at low gravity because of decreased opacity from these refractory species, while VO bands are stronger (see, e.g., Kirkpatrick et al. 2006). The 1.17um VO band is not used as a gravity indicator at low resolution because if is blended with K I, FeH and H_2O (Allers & Liu 2013). Collision-induced absorption from molecular hydrogen (H_2 CIA) also changes as a function of gravity, with lower collision rates in low-gravity objects imparting a triangular shape to the H band.

Several prior analyses have introduced broad-band measures to discern low-gravity from field-gravity objects. Allers & Liu (2013) design several near-IR indices to measure the changing strengths of FeH, VO, and K I absorption and the slope of the H-band continuum as a func-

tion of gravity by comparing ∼1-100 Myr M5-L7 members of young moving associations with field dwarfs. Canty et al. (2013) analyzed M9-L0 dwarfs to design an $H_2(K)$ index that measures the contribution of H_2 CIA on the slope of the K-band continuum; Schneider et al. (2014) expand this index to the L dwarfs. Indices have the potential to offer a quantitative gravity classification, analogous to spectral classification. However, index measures depend on the spectral resolution of the data used to calibrate them, and our spectra are sufficiently distinct from those used in prior studies. In addition, most of the indices do not extend into the late-L dwarfs, and so are inadequate to classify some of our most interesting objects. Therefore, we do not adopt spectral indices as a default gravity classification scheme. However, we do check for consistency with applicable spectral indices whenever we note peculiarities in the spectra of our L and T candidates.

We note that some of the spectral features, in particular the strength of the FeH bands, the peakiness of the H-band continuum, and the redness of the near-IR SED, may also be attributable to high atmospheric dust content or thicker clouds, as discussed in Looper et al. (2008b) and Allers & Liu (2013). High dust content itself may be linked to low gravity, so a clear distinction may not always be possible, especially at low spectral resolution.

Our assessment of peculiarity is based on two factors: (1) the deviation from the median J-Ks colors for objects of the same spectral type, with $>2\sigma$ outliers considered peculiar, or (2) high spectral similarity to objects that have previously been classified as peculiar. In two cases below (Sections 4.2.2–4.2.3), we find similarities to the spectra of objects previously classified as peculiar because of being young and/or dusty. In the remaining two cases (Sections 4.2.1 and 4.2.4) the assessment of peculiarity is based on the comparison to spectra of previously classified peculiar objects as well as the $J - K_s$ colors.

4.2.1. 2MASS J11193254−1137466 (L7)

The most interesting object uncovered by our cross-correlation is 2M 1119−1137. This object is one of the reddest objects published to date with a synthetic $J - K_s = 2.62 \pm 0.15$ mag. Only the L7 dwarfs PSO J318.5338−22.8603 (Liu et al. 2013) and ULAS J222711−004547 (Marocco et al. 2014) among free-floating brown dwarfs are known to be redder. From its low-resolution spectrum (Figure 4), we classify this object as an L7. The low signal-to-noise prevents us from unambiguously determining if this object has low gravity. The peak of the H-band continuum — thought to be sharpened at low surface gravity (e.g., Lucas et al. 2001; Allers & Liu 2013) — is not very sharp. We measured the H-cont index of Allers & Liu (2013) and found a value of 0.907, which is 1.5σ above the medan for L7 dwarfs, and similar to the H-cont indices of low gravity objects. The authors note that very red L dwarfs with no youth signatures can still exhibit a triangular H-band shapes and similarly high H-cont indices. In summary, the H-cont index of 2M 1119−1137 is consistent with it being a low-gravity object, but we can not conclude from the index alone that it is definitely young.

In Figure 5 we compare 2M 1119−1137 to the known very low-gravity dwarfs 2MASSW J224431.67+204343.3 (L7.5; Looper et al. 2008a), WISE J174102.78−464225.5 (L7; Schneider et al. 2014), and WISEP J004701.06+680352.1 (L7.5; Gizis et al. 2012). We see that 2M1119−1137 most closely matches W0047+6803 and also matches the redness of W1741−4642 but has a less peaked H-band and a shallower slope in the K-band. Although it is slightly redder, the shape of the H- and K-band of 2M 1119−1137 also matches that of 2M 2244+2043. The agreement with the spectra of other young L7–L7.5 dwarfs also indicate that 2M 1119−1137 may be young. A decisive classification will require higher-SNR and/or higher-resolution spectra than we presently have.

Further evidence that 2M 1119−1137 may be young comes from its proper motion and photometric distance. By comparing the 2MASS and AllWISE positions, we estimate an annual proper motion of -155 ± 20 mas in right ascension and -101 ± 17 mas in declination. Given a K_s absolute magnitude of 12.6 ± 0.4 mag for young L7 dwarfs or 12.5 ± 0.4 mag for field-age L7 dwarfs (calculated from the empirically determined $L_{\rm bol}$-SpT relationship and K_s bolometric corrections from Filippazzo et al. 2015), the photometric parallax of 2M 1119−1137 is 40 ± 12 mas or 38 ± 12 mas. The BANYAN II space motion estimation algorithm (Malo et al. 2013; Gagné et al. 2014) gives 2M 1119−1137 between 39% and 69% probability of being a TW Hydrae moving group member, depending on whether an arbitrary age or a <1 Gyr age is chosen as an input prior with the respective photometric parallax estimates. Confirmation of the association with the TW Hydrae group will require radial velocity and trigonometric parallax measurements.

Should 2M 1119−1137 be confirmed as a member of the 7–13 Myr (Bell et al. 2015) TW Hydrae association (Webb et al. 1999), it will be its coolest and lowest-mass (5–6 $M_{\rm Jup}$, based on evolutionary models by Allard et al. 2012) free-floating member. Only the planetary-mass companion 2M 1207b (Chauvin et al. 2004, 2005) is likely cooler.

4.2.2. 2MASS J17081563+2557474 (L5)

This object is determined to be a young L5 brown dwarf based on the decreased absorption of K I and FeH and the increased absorption of H_2O in the J-band. Calculations of the spectral indices from Allers & Liu (2013) and Schneider et al. (2014) also suggest that this object is a low gravity brown dwarf. As seen in Figure 4, the strengths of the gravity sensitive features in the J-band and the shape of the H-band are more similar to the young L5 2MASS J23174712-4838501 (Kirkpatrick et al. 2010), although the observed spectrum is still slightly redder than the comparison spectrum.

4.2.3. 2MASS J16135698+4019158 (L5)

While this object is peculiarly red, it does not exhibit the features of a low-gravity object. As seen in Figure 4, the object has normal absorption strengths, aside from H_2O, and is more similar to the red L5 dwarf 2M 2351+3010 published in Kirkpatrick et al. (2010). There is also strong FeH

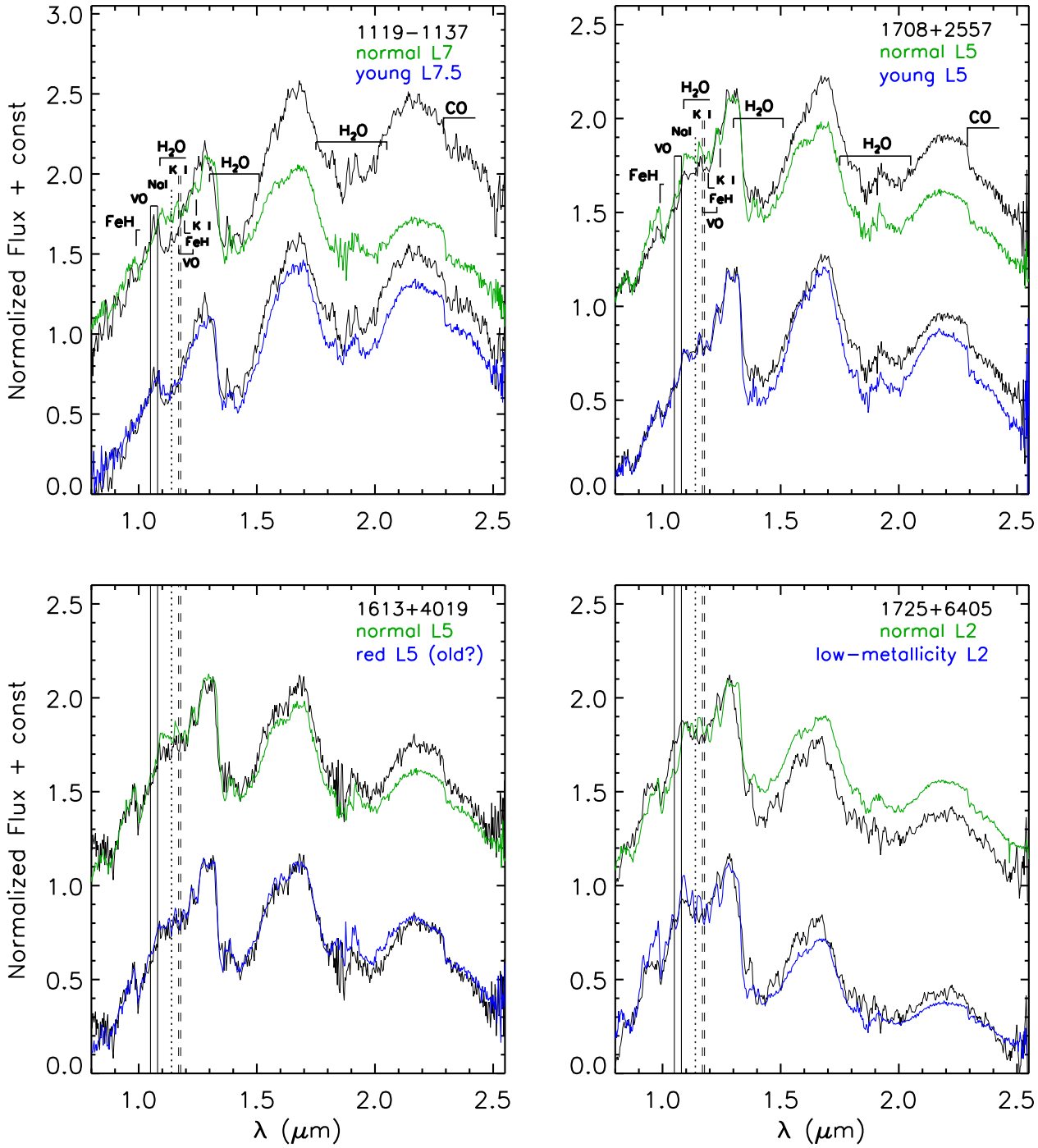

Fig. 4.— Spectra of the four peculiar objects identified in this work. In each case, the spectrum of the candidate is compared to the spectrum of a normal object of the same spectral type, and to the spectrum of a peculiar object of the nearest spectral type. The comparison spectra from left to right and top to bottom are L7 (2MASS J0028208+224905; Burgasser et al. 2010) and L7.5 young (2MASS J22443167+2043433; Looper et al. 2008a); L5 (2MASS J01550354+0950003; Burgasser et al. 2010) and L5 pec (2MASS J23174712−4838501; Kirkpatrick et al. 2010); L5 (2MASS J01550354+0950003; Burgasser et al. 2010) and L5 pec (2MASS J23512200+3010540; Kirkpatrick et al. 2010); L2 (2MASS J13054019−2541059; Burgasser et al. 2007) and L2 pec (2MASS J14313097+1436539; Sheppard & Cushing 2009).

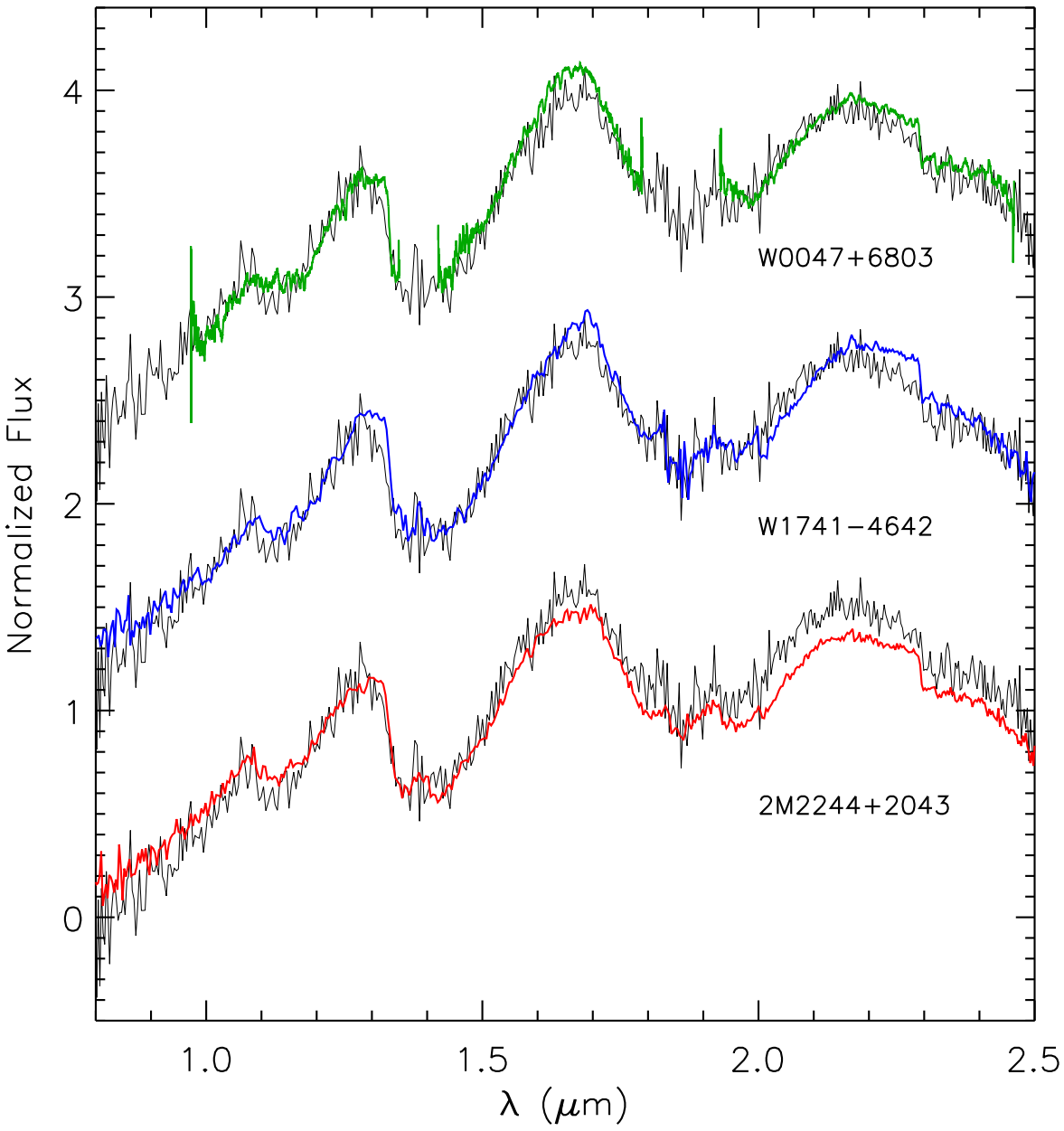

Fig. 5.— A comparison of the SpeX prism spectrum of 2M 1119−1137 (black) with low-resolution spectra of other young L7–L7.5 dwarfs: WISEP J004701.06+680352.1 (L7.5 (pec), Gizis et al. 2012), WISE J174102.78−464225.5 (L7 (pec), Schneider et al. 2014) and 2MASSW J224431.67+204343.3 (L7.5 (pec), Kirkpatrick et al. 2010).

absorption. The authors speculate that 2M 2351+3010 is actually an older object that simply has a higher dust content. Since our object seems very similar in nature, we adopt this explanation as well.

4.2.4. 2MASS J17251557+6405005 (L2)

2M 1725+6405 is a peculiarly blue L2 dwarf (Fig. 4). This object was found in our cross-correlation but it was not part of our high-priority sample. Peculiarly blue L dwarfs have often been classified as metal-poor (e.g., Burgasser et al. 2003; Burgasser 2004), with their blue near-IR colors dictated by increasingly strong collision-induced hydrogen absorption over 1.5–2.5 μm. Metal-poor L dwarfs, or L subdwarfs, also show strong metal-hydride absorption. However, the FeH Wing-Ford band at 0.99 μm in 2M 1725+6405 is weak compared to the standard, which suggests that the 2M 1725+6405 is blue likely because it is unusually dust-poor.

It is also possible that 2M 1725+6405 may be an unresolved L + T dwarf binary, with the J band flux enhanced by the T dwarf component. We consider unresolved binarity in the next Section (4.3). Unlike all of the candidate binaries discussed in Section 4.3, we actually do not find a better binary template fit for 2M 1725+6405. We therefore conclude that this L2 dwarf is intrinsically blue.

4.3. Brown Dwarfs with Composite Spectral Types

Several of the objects show peculiarities that do not readily match those found in other individual objects. Instead, they more closely resemble combination spectra of L and T dwarfs. Burgasser (2007) and Burgasser et al. (2010) developed a technique that enables one to infer the spectral types of the individual components of a candidate unresolved binary by a goodness-of-fit comparison to a library of spectral template combinations. We adopt this technique in a simple form, by creating combination templates from the set of single L and T dwarf standards from the SpeX Prism Library. Unlike Burgasser et al. (2010), we do not create a large list of templates built on the entire population of L and T dwarfs with available SpeX spectra. Nonetheless, we find that our simple approach gives sufficient indication whether a brown dwarf displays a composite spectral signature, and produces approximate spectral types for the components.

Our composite template spectra are constructed by normalizing all of the standard single brown dwarfs over the same wavelength range (1.2-1.3 μm; chosen because it is relatively free of absorption features), scaling them to their absolute spectral-type dependent magnitudes given by the polynomials in Table 14 of Dupuy & Liu (2012), and summing the pairs of resulting spectra. We compute the χ^2 over most of the 0.8-2.5 μm region, excluding ranges of strong water absorption (1.35-1.45 and 1.8-2.0 μm). In all cases, the χ^2 is greater than one but this is to be expected as we are only testing the fit to templates created from one object of each spectral type. We have

classified an object as a likely spectral type composite – a potential binary – if the χ^2 of the dual-template spectral fit is significantly lower than the χ^2 of the single-template fit. Each of the χ^2 values have been calculated over the entire 0.8-2.5 μm region, minus the water absorption bands.

In addition to template fitting, we have analyzed the spectral indices defined specifically for SpeX prism spectra in Burgasser et al. (2010) for all our binary candidates and we report the strength of their candidate binarity. We have also analyzed the SpeX prism spectral indices from Bardalez Gagliuffi et al. (2014) but because the binary index selection criteria in that work were not designed for late-L to early-T dwarfs, we only report the results where applicable.

We note that while brown dwarfs displaying combination spectral signatures have until recently been considered to all be unresolved binaries, they can also be highly variable brown dwarfs with photospheres that display two distinct temperature components. Recent examples include the T1.5 dwarf 2MASS J21392676+0220226, suggested as a strong L8.5 + T3.5 spectral binary candidate by Burgasser et al. (2010), but identified as a J-band variable that is unresolved in *HST* images (Radigan et al. 2012), or the T dwarfs 2MASS J13243559+6358284 (T2.5) and SDSS J151114.66+060742.9 (T2), identified as binary candidates (Burgasser et al. 2010; Geißler et al. 2011), but that are also unresolved in *HST* and are variable (Metchev et al. 2015). Therefore, while the objects discussed in this section are considered candidate unresolved binaries, they are also strong candidates for photometric variables.

4.3.1. 2MASS J13043568+1542521 (L6+T6?)

This object is one of several that is best fit by a binary combination template. As seen in Figure 6, the best fit single brown dwarf (T0) does not match the features of 2M 1304+1542. The Y-/J-band ratio is lower than any of the closest standard objects and the H-band has a dip at $\sim$1.65 μm. The K-band does not have differences that are as pronounced as in the other bands though it is slightly redder than the standard object. In fitting this object with a binary template, we find that the best fit is a combination of an L6 and a T6 brown dwarf. The Y-/J-band ratio and the K-band flux more closely resemble the object spectrum. The contribution of the methane break in the cooler brown dwarf at 1.6 μm also reproduces the dip in the H-band well. Further evidence that this object is a binary comes from the analysis of spectral indices identified in Burgasser et al. (2010) and Bardalez Gagliuffi et al. (2014). 2M 1304+1542 satisfies four of the six binary index selection criteria given in Table 5 of Burgasser et al. (2010) and ten of the twelve selection criteria in Table 4 of Bardalez Gagliuffi et al. (2014), making this a strong binary candidate.

4.3.2. 2MASS J14025564+0800553 (L8+T5?)

The spectrum of 2M 1402+0800 also shows distinctive composite characteristics. While the Y-/J-band ratio is not significantly dissimilar from the closest single brown dwarf spectrum, the

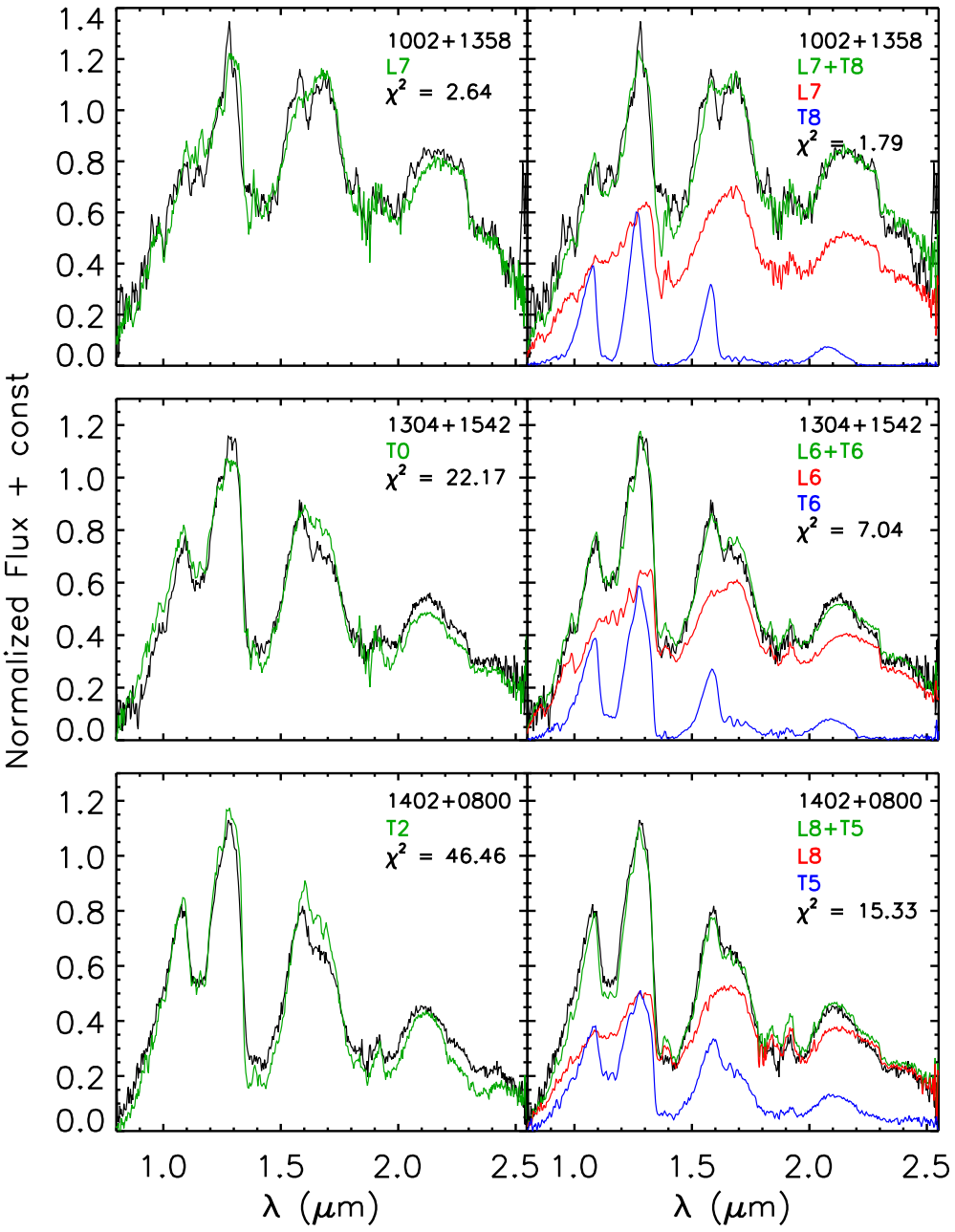

Fig. 6.— Spectra of all objects identified as candidate unresolved binaries (or photometric variables). The left panels show comparisons to the spectra (in green) that fit the 0.95-1.35 μm continuum best: i.e., as done for spectral typing of the individual objects in Sections 4.1–4.2. The right panels show the two-component templates (also in green) that fit best over 0.8-2.5 μm; the individual component contributions are shown in red and blue. The quoted χ^2 values are the smallest ones for, respectively, single- and binary-template fits over the entire 0.8-2.5 μm range, as done in Section 4.3. The comparison spectra from left to right and top to bottom are: L7 (2MASS J0028208+224905; Burgasser et al. 2010) and T8 (2MASS J04151954-0935066; Burgasser et al. 2004); T0 (2MASS J12074717+0244249; Looper et al. 2007), L6 (2MASS J10101480-0406499; Reid et al. 2006) and T6 (2MASS J16241436+0029158; Burgasser et al. 2006a); T2 (2MASS J12545393-0122474; Burgasser et al. 2004), L8 (2MASS J16322911+1904407; Burgasser 2007) and T5 (2MASS J15031961+2525196; Burgasser et al. 2004).

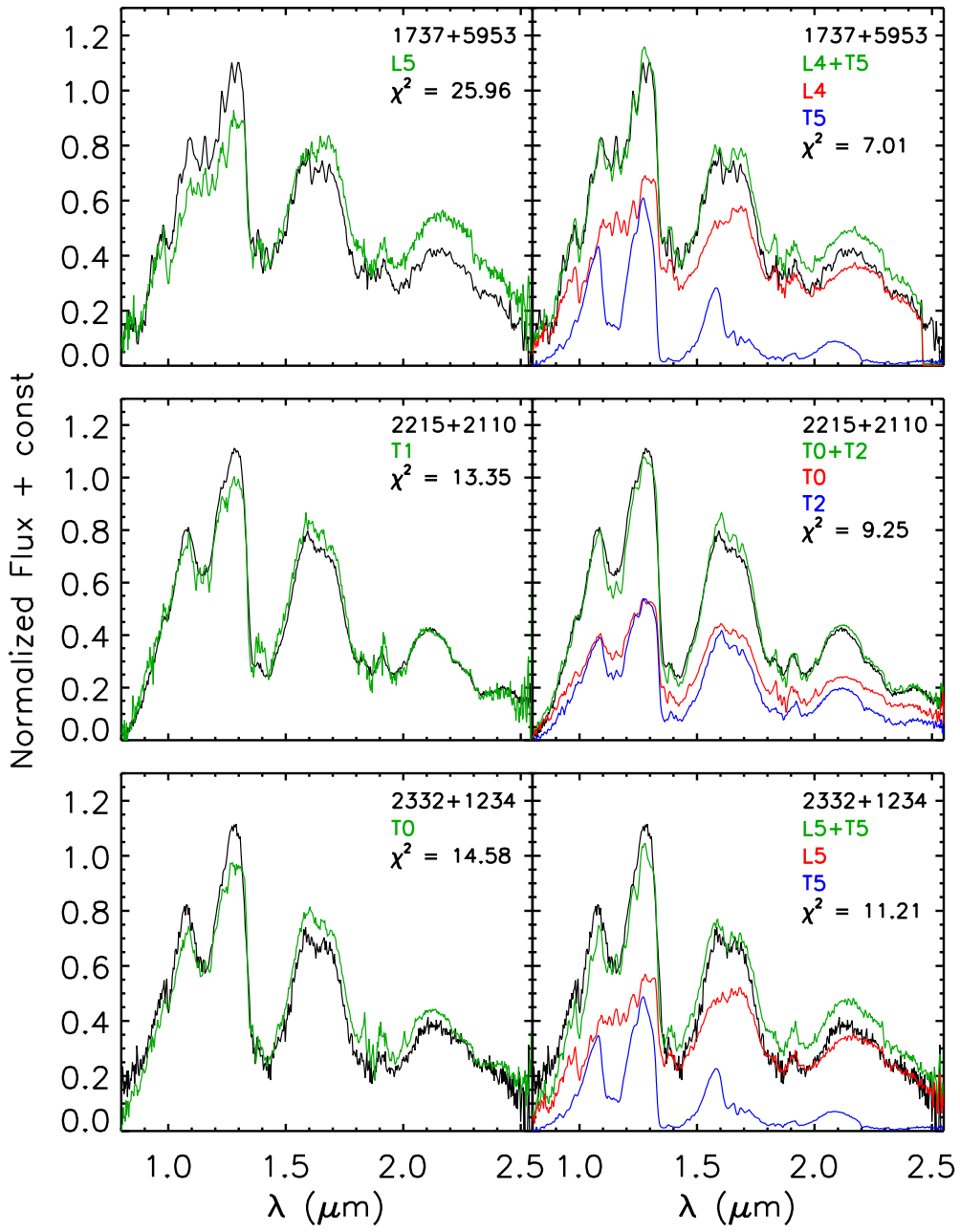

Fig. 6 (cont).— The comparison spectra from left to right and top to bottom are: L5 (2MASS J08350622+1953050; Chiu et al. 2006), L4 (2MASS J21580457-1550098; Kirkpatrick et al. 2010) and T5 (2MASS J15031961+2525196; Burgasser et al. 2004); T1 (2MASS J01514155+1244300; Burgasser et al. 2004), T0 (2MASS J12074717+0244249; Looper et al. 2007) and T2 (2MASS J12545393-0122474; Burgasser et al. 2004). L5 (2MASS J08350622+1953050; Chiu et al. 2006) and T5 (2MASS J15031961+2525196; Burgasser et al. 2004).

H- and K-bands are more similar to an L8+T5 binary. Figure 6 shows that the shape and relative flux of all three 2MASS bandpasses are very well reproduced by the L/T binary template. Most importantly, the dip in the H-band is well reproduced by the contribution of the methane in the T dwarf. This object passes all six of the binary index selection criteria of Burgasser et al. (2010) which makes it a strong binary candidate.

4.3.3. 2MASS J17373467+5953434 (L4+T5?)

This object is classified as having an L4+T5 composite spectrum. As seen in Figure 6, an L5 spectrum matches 2M 1737+5953 well in the Y- and J-bands but is a very poor match to the H- and K-bands. The observed spectrum shows signs of methane absorption at 1.6 and 2.2 μm which is indicative of having a T dwarf secondary component. The binary index selection criteria from Burgasser et al. (2010) were not designed for mid-L dwarfs so we analyzed the spectral indices from Bardalez Gagliuffi et al. (2014) instead. Because this object only passes four of the twelve selection criteria from Bardalez Gagliuffi et al. (2014), it is only a weak binary candidate.

4.3.4. 2MASS J23322678+1234530 (L5+T5?)

While 2M 2332+1234 is best fit in the J-band by a scaled T0 spectrum, the H- and K-bands clearly do not appear to belong to a T0 dwarf. The H-band shows evidence of methane absorption at 1.6-1.8 μm but there is less presence of CH_4 in the K-band. This points to a composite L/T spectrum similar to SDSS J151114.66+060742.9 presented in Burgasser et al. (2010). The methane absorption features are best fit by an L5+T5 template, however, the continuum of our observed spectrum is still slightly bluer at the longer wavelengths. This object passes four of the binary index selection criteria of Burgasser et al. (2010) which makes it a strong binary candidate.

4.3.5. 2MASS J10020752+1358556 (L7+T8?)

This object is tentatively classified as having a composite spectrum. As seen in Figure 6, 2M 1002+1358 has a large dip in flux in the H band at the location of the CH_4 absorption feature that is usually present in a T dwarf, and has much more water and methane absorption in the J-band than a typical L dwarf. The K- band, however, seems to be similar to an L4–L6 dwarf. These suggest a composite spectral type. There is a much greater difference between L and T dwarfs in the J- and H-band features than there is in the K-band features, therefore, the K-band of a combined binary spectrum can look like it belongs to an L dwarf whereas the J- and H-bands will appear to have a contribution from both binary components. The large dip in H-band flux may also be the result of an extraneous signal in the raw spectrum of the object as it has an atypical shape compared to that of a feature usually associated with CH_4. However, the spectrum of the

telluric calibration star does not exhibit the same behavior, while the feature is apparent in most of the individual spectra of this object, even if at low SNR. This suggests that the feature may be real, even if we can not fully exclude a random variation due to noise. Analyzing the spectral indices does not shed any light on the true nature of this object as it only passes four of the twelve binary index selection criteria from Bardalez Gagliuffi et al. (2014), making it a weak binary candidate.

4.3.6. 2MASS J22153705+2110554 (T0+T2?)

The T dwarf 2M 2215+2110 is a new discovery in the SDSS footprint. Some of the features in the spectrum of 2M 2215+2110 are ambiguous as to their origin. While the J- and K- bands more closely resemble an early T dwarf, the H- band has a clear dearth of flux. The overall shape of this band might be explained by a presence of a slightly later-type T dwarf secondary component than the primary, but the lack of flux still persists in the binary template spectrum. Several features, such as the FeH feature at 0.99 μm, do match a T0+T2 composite spectrum. However, the H_2O + CH_4 absorption between 1.1–1.2 μm is much stronger in the binary composite template than in the observed spectrum. The spectral indices also do not help us with this object – only two of the index selection criteria from Burgasser et al. (2010) are passed which makes this object a weak binary candidate.

5. Discussion

Our search was aimed at discovering peculiar L or T dwarfs, with priority in this first iteration placed on unusually red objects. Overall, we have observed and identified 10 peculiar or binary L dwarfs, 16 normal L dwarfs, one T dwarf, and 13 M dwarfs. The latter had been mis-identified as candidate L or T dwarfs because of low-SNR photometry.

The total fraction of objects in an unbiased sample of brown dwarfs with $J - K_s$ colors $>2\sigma$ from the mean color at a given spectral type — the criterion used for detecting photometrically peculiar L and T dwarfs in Faherty et al. (2009) — is expected to be 4.6%. Faherty et al. (2009) report a somewhat larger fraction, 5.8%, of peculiar objects among the 1268 M7–T8 dwarfs in their sample. The small discrepancy arises from an apparent non-gaussianity of the $J - K_s$ color distribution: they have nearly twice as many red outliers than blue outliers.

Only three of our L dwarfs are peculiarly red or dusty, and an equal number of our discoveries are in fact peculiarly blue. While at face value this does not indicate a higher success rate in finding peculiarly red objects than in a random sample of field brown dwarfs, we have at present followed up only a small number (40) of our total candidate sample (314). The 40 objects presented here comprise roughly equal numbers of high- (22) and low-priority (18) objects: a circumstance of weather and observational constraints. It is possible that the larger high-priority sample (178 candidates) will reveal a higher incidence rate of unusually red objects.

We do find, however, that our present prioritization strategy reveals a larger fraction of unusual objects — including not only peculiar L dwarfs but also candidate unresolved binaries that are not color outliers in $J - K_s$ but are unusually red in $z - J$ — among the high-priority candidates. Eight of the 22 objects in the high-priority sample are peculiar or candidate binaries vs. two of the 18 in the low-priority sample. The difference between the two is statistically significant at the 96% level. It indicates that combinations of optical and infrared colors, such as employed here, can successfully discern even moderate peculiarities in ultra-cool dwarfs. Table 3 summarizes the peculiarities of each object — from spectral comparison and synthetic colors.

Because L and T dwarfs are brighter in the 3–5 μm wavelength range, we investigated whether the $J-K_s$ color outliers also have unusual colors at these wavelengths. We find that L dwarfs with the very reddest $J - K_s$ colors are clearly distinguishable from the locus of L dwarfs on a $J - K_s$ vs. $H - W2$ and $J - K_s$ vs. $W1 - W2$ diagram (Fig. 7) mainly because of their red near-IR colors. They stand out in their $J - K_s$ and $H - W2$ colors but not significantly in their $W1 - W2$ colors. T dwarfs with peculiarly red $J - K_s$ colors are only marginally redder in $H - W2$ and $W1 - W2$, and the peculiarly blue L or T dwarfs are not distinguishable from the normal population with the exception of the blue L dwarf discovered in this work (2MASS J17251557+6405005).

6. Conclusions

We performed a color-selected search for peculiar L and T dwarfs, focusing primarily on the peculiarly red objects, and demonstrated that with the proper selection criteria, we can identify unusual L and T dwarf candidates in large photometric surveys in the absence of spectral type information. With follow-up spectroscopy, we can verify the unusual properties and begin to discern their underlying cause. This is particularly advantageous for finding isolated objects that are analogous to the typically very red directly imaged extrasolar planets in order to study their atmospheric characteristics at higher fidelity. We had a high success rate in discovering either peculiar L dwarfs or candidate unresolved binaries in our prioritized sample, and discovered one of the reddest L dwarfs known to date. This new red L7 dwarf is a potential TW Hydrae member, and if confirmed, would make it the coolest and least massive free-floating object in the association. We note that even after many searches for T dwarfs in the SDSS and 2MASS catalogs, we still uncovered a new T dwarf among the ∼13% fraction of candidates that we have spectroscopically characterized so far. These discoveries attest to the power of simultaneous positional and color cross-correlations across photometric databases — as performed here, in Metchev et al. (2008), in Geißler et al. (2011), and now enabled with the Virtual Astronomical Observatory — over color-only searches on individual databases that are then positionally compared to other databases. At the same time, the discovery of only a single new T dwarf in our characterized sample indicates the census of T dwarfs (132) in SDSS is nearly complete.

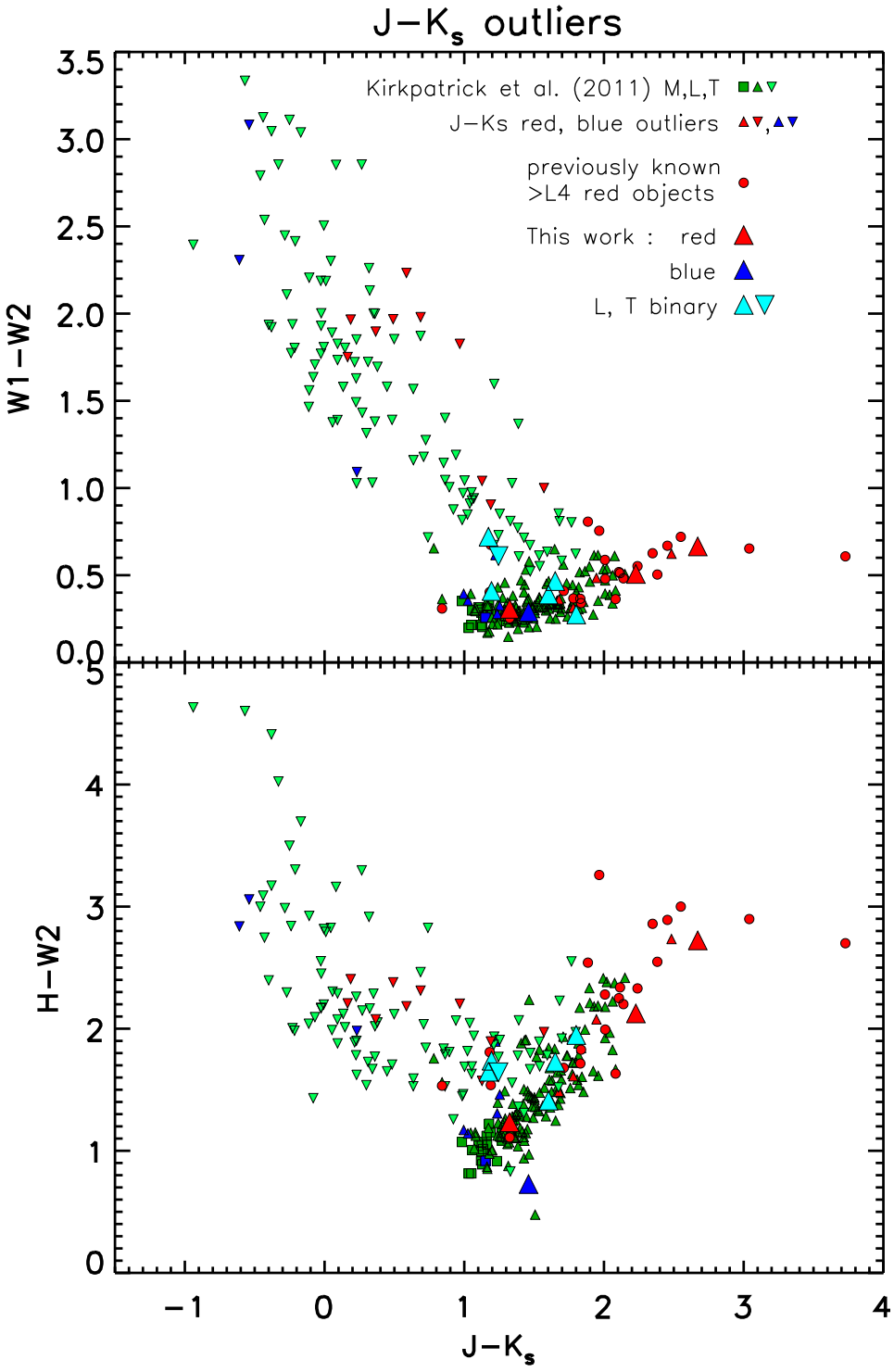

Fig. 7.— Photometric color-color diagrams of objects from Kirkpatrick et al. (2011). Upwards and downwards triangles denote L and T dwarfs, respectively. Red symbols denote objects with $J-K_s$ colors $>2\sigma$ redder than the mean for their spectral type Faherty et al. (2009, 2013). Blue symbols denote objects that are $>2\sigma$ bluer. Large symbols represent peculiar objects identified in this work. Red circles indicate the previously known red brown dwarfs with spectral types of L4 and later.

REFERENCES

Ahn, C. P., Alexandroff, R., Allende Prieto, C., et al. 2012, ApJS, 203, 21

Allard, F., Homeier, D., & Freytag, B. 2012, Philosophical Transactions of the Royal Society of London Series A, 370, 2765

Aller, K. M., Kraus, A. L., Liu, M. C., et al. 2013, ApJ, 773, 63

Allers, K. N., & Liu, M. C. 2013, ApJ, 772, 79

Allers, K. N., Jaffe, D. T., Luhman, K. L., et al. 2007, ApJ, 657, 511

Bardalez Gagliuffi, D. C., Burgasser, A. J., Gelino, C. R., et al. 2014, ApJ, 794, 143

Bell, C. P. M., Mamajek, E. E., & Naylor, T. 2015, MNRAS, 454, 593

Bochanski, J. J., Hennawi, J. F., Simcoe, R. A., et al. 2009, PASP, 121, 1409

Bonnefoy, M., Boccaletti, A., Lagrange, A.-M., et al. 2013, A&A, 555, A107

Burgasser, A. J. 2004, ApJ, 614, L73

—. 2007, ApJ, 659, 655

Burgasser, A. J., Burrows, A., & Kirkpatrick, J. D. 2006a, ApJ, 639, 1095

Burgasser, A. J., Cruz, K. L., Cushing, M., et al. 2010, ApJ, 710, 1142

Burgasser, A. J., Geballe, T. R., Leggett, S. K., Kirkpatrick, J. D., & Golimowski, D. A. 2006b, ApJ, 637, 1067

Burgasser, A. J., Liu, M. C., Ireland, M. J., Cruz, K. L., & Dupuy, T. J. 2008, ApJ, 681, 579

Burgasser, A. J., Looper, D. L., Kirkpatrick, J. D., & Liu, M. C. 2007, ApJ, 658, 557

Burgasser, A. J., McElwain, M. W., Kirkpatrick, J. D., et al. 2004, AJ, 127, 2856

Burgasser, A. J., Kirkpatrick, J. D., Burrows, A., et al. 2003, ApJ, 592, 1186

Canty, J. I., Lucas, P. W., Roche, P. F., & Pinfield, D. J. 2013, MNRAS, 435, 2650

Chauvin, G., Lagrange, A.-M., Dumas, C., et al. 2004, A&A, 425, L29

—. 2005, A&A, 438, L25

Chiu, K., Fan, X., Leggett, S. K., et al. 2006, AJ, 131, 2722

Cruz, K. L., Kirkpatrick, J. D., & Burgasser, A. J. 2009, AJ, 137, 3345

Cushing, M. C., Vacca, W. D., & Rayner, J. T. 2004, PASP, 116, 362

Cutri, R. 2006, 2MASS All-Sky Data Release Explanatory Supplement: Full Survey Image Atlas and Source "Reject" Tables; Cautionary Notes, `http://www.ipac.caltech.edu/2mass/releases/allsky/doc/seca2_1c.html`, [Online; accessed 26-October-2013]

Dupuy, T. J., & Liu, M. C. 2012, ApJS, 201, 19

Faherty, J. K., Burgasser, A. J., Cruz, K. L., et al. 2009, AJ, 137, 1

Faherty, J. K., Rice, E. L., Cruz, K. L., Mamajek, E. E., & Núñez, A. 2013, AJ, 145, 2

Faherty, J. K., Burgasser, A. J., Walter, F. M., et al. 2012, ApJ, 752, 56

Filippazzo, J. C., Rice, E. L., Faherty, J., et al. 2015, ApJ, 810, 158

Gagné, J., Lafrenière, D., Doyon, R., Malo, L., & Artigau, É. 2014, ApJ, 783, 121

—. 2015, ApJ, 798, 73

Geißler, K., Metchev, S., Kirkpatrick, J. D., Berriman, G. B., & Looper, D. 2011, ApJ, 732, 56

Gizis, J. E., Faherty, J. K., Liu, M. C., et al. 2012, AJ, 144, 94

Golimowski, D. A., Leggett, S. K., Marley, M. S., et al. 2004, AJ, 127, 3516

Gorlova, N. I., Meyer, M. R., Rieke, G. H., & Liebert, J. 2003, ApJ, 593, 1074

Horne, K. 1986, PASP, 98, 609

Kirkpatrick, J. D., Barman, T. S., Burgasser, A. J., et al. 2006, ApJ, 639, 1120

Kirkpatrick, J. D., Reid, I. N., Liebert, J., et al. 2000, AJ, 120, 447

Kirkpatrick, J. D., Looper, D. L., Burgasser, A. J., et al. 2010, ApJS, 190, 100

Kirkpatrick, J. D., Cushing, M. C., Gelino, C. R., et al. 2011, ApJS, 197, 19

Knapp, G. R., Leggett, S. K., Fan, X., et al. 2004, AJ, 127, 3553

Liu, M. C., Magnier, E. A., Deacon, N. R., et al. 2013, ApJ, 777, L20

Lodieu, N., Hambly, N. C., Jameson, R. F., & Hodgkin, S. T. 2008, MNRAS, 383, 1385

Looper, D. L., Gelino, C. R., Burgasser, A. J., & Kirkpatrick, J. D. 2008a, ApJ, 685, 1183

Looper, D. L., Kirkpatrick, J. D., & Burgasser, A. J. 2007, AJ, 134, 1162

Looper, D. L., Kirkpatrick, J. D., Cutri, R. M., et al. 2008b, ApJ, 686, 528

Lucas, P. W., Roche, P. F., Allard, F., & Hauschildt, P. H. 2001, MNRAS, 326, 695

Luhman, K. L., & Sheppard, S. S. 2014, ApJ, 787, 126

Lupton, R. H., Ivezic, Z., Gunn, J. E., et al. 2002, in Society of Photo-Optical Instrumentation Engineers (SPIE) Conference Series, Vol. 4836, Survey and Other Telescope Technologies and Discoveries, ed. J. A. Tyson & S. Wolff, 350–356

Malo, L., Doyon, R., Lafrenière, D., et al. 2013, ApJ, 762, 88

Marley, M. S., Saumon, D., Cushing, M., et al. 2012, ApJ, 754, 135

Marocco, F., Day-Jones, A. C., Lucas, P. W., et al. 2014, MNRAS, 439, 372

McGovern, M. R., Kirkpatrick, J. D., McLean, I. S., et al. 2004, ApJ, 600, 1020

McLean, I. S., Prato, L., McGovern, M. R., et al. 2007, ApJ, 658, 1217

Metchev, S. A., Kirkpatrick, J. D., Berriman, G. B., & Looper, D. 2008, ApJ, 676, 1281

Metchev, S. A., Heinze, A., Apai, D., et al. 2015, ApJ, 799, 154

Press, W. H., Teukolsky, S. A., Vetterling, W. T., & Flannery, B. P. 1992, Numerical recipes in FORTRAN. The art of scientific computing

Radigan, J., Jayawardhana, R., Lafrenière, D., et al. 2012, ApJ, 750, 105

Rayner, J. T., Toomey, D. W., Onaka, P. M., et al. 2003, PASP, 115, 362

Reid, I. N., Lewitus, E., Burgasser, A. J., & Cruz, K. L. 2006, ApJ, 639, 1114

Rice, E. L., Barman, T., Mclean, I. S., Prato, L., & Kirkpatrick, J. D. 2010, ApJS, 186, 63

Robertson, J. G. 1986, PASP, 98, 1220

Schmidt, S. J., West, A. A., Hawley, S. L., & Pineda, J. S. 2010, AJ, 139, 1808

Schneider, A. C., Cushing, M. C., Kirkpatrick, J. D., et al. 2014, AJ, 147, 34

Sheppard, S. S., & Cushing, M. C. 2009, AJ, 137, 304

Simcoe, R. A., Burgasser, A. J., Bernstein, R. A., et al. 2008, in Society of Photo-Optical Instrumentation Engineers (SPIE) Conference Series, Vol. 7014, Society of Photo-Optical Instrumentation Engineers (SPIE) Conference Series

Vacca, W. D., Cushing, M. C., & Rayner, J. T. 2003, PASP, 115, 389

Vrba, F. J., Henden, A. A., Luginbuhl, C. B., et al. 2004, AJ, 127, 2948

Webb, R. A., Zuckerman, B., Platais, I., et al. 1999, ApJ, 512, L63

Yasuda, N., Fukugita, M., Narayanan, V. K., et al. 2001, AJ, 122, 1104

Zhang, Z. H., Pokorny, R. S., Jones, H. R. A., et al. 2009, A&A, 497, 619

Facilities: IRTF (SpeX spectrograph), Magellan: Baade (FIRE spectrograph)

We would like to thank our referee, Jackie Faherty, for her insightful critique.

This work was supported by the NASA Astrophysical Data Analysis Program through award No. NNX11AB18G to S.M. at Stony Brook University and by an NSERC Discovery grant to S.M. at The University of Western Ontario. Part of the data are obtained with the Magellan-Baade 6.5m telescope under program CN2012A-54. Support for R.K. is provided from Fondecyt Reg. No. 1130140 and by the Ministry of Economy, Development, and Tourisms Millennium Science Initiative through grant IC12009, awarded to The Millennium Institute of Astrophysics (MAS). The authors wish to recognize and acknowledge the very significant cultural role and reverence that the summit of Mauna Kea has always had within the indigenous Hawaiian community. We are most fortunate to have the opportunity to conduct observations from this mountain. This paper includes data gathered with the 6.5 meter Magellan Telescopes located at Las Campanas Observatory, Chile. This publication makes use of data products from the Two Micron All Sky Survey, which is a joint project of the University of Massachusetts and the Infrared Processing and Analysis Center/California Institute of Technology, funded by the National Aeronautics and Space Administration and the National Science Foundation. Funding for SDSS-III has been provided by the Alfred P. Sloan Foundation, the Participating Institutions, the National Science Foundation, and the U.S. Department of Energy Office of Science. The SDSS-III web site is http://www.sdss3.org/. SDSS-III is managed by the Astrophysical Research Consortium for the Participating Institutions of the SDSS-III Collaboration including the University of Arizona, the Brazilian Participation Group, Brookhaven National Laboratory, Carnegie Mellon University, University of Florida, the French Participation Group, the German Participation Group, Harvard University, the Instituto de Astrofisica de Canarias, the Michigan State/Notre Dame/JINA Participation Group, Johns Hopkins University, Lawrence Berkeley National Laboratory, Max Planck Institute for Astrophysics, Max Planck Institute for Extraterrestrial Physics, New Mexico State University, New York University, Ohio State University, Pennsylvania State University, University of Portsmouth, Princeton University, the Spanish Participation Group, University of Tokyo, University of Utah, Vanderbilt University, University of Virginia, University of Washington, and Yale University. This publication makes use of data products from the Wide-field Infrared Survey Explorer, which is a joint project of the University of California, Los Angeles, and the Jet Propulsion Laboratory/California Institute of Technology, funded by the National Aeronautics and Space Administration. This research has made use of data obtained from or software provided by the US Virtual Astronomical Observatory,

This preprint was prepared with the AAS LaTeX macros v5.2.

which is sponsored by the National Science Foundation and the National Aeronautics and Space Administration.